

**Operational and Investment Solutions to Enhance the Transmission and  
Distribution Systems of the Electrical Grid**

by

Ebrahim Mortaz

A dissertation submitted to the Graduate Faculty of  
Auburn University  
in partial fulfillment of the  
requirements for the Degree of  
Doctor of Philosophy

Auburn, Alabama

August 5, 2017

Keywords: Power transmission, Power distribution, Microgrid, Electric vehicles,  
Optimization, Economics

Copyright 2017 by Ebrahim Mortaz

Approved by

Jorge Valenzuela, Chair, Professor of Industrial and Systems Engineering  
Robert “Glenn” Richey Jr., Professor of Aviation and Supply Chain Management  
Alexander Vinel, Assistant Professor of Industrial and Systems Engineering  
Fadel Megahed, Assistant Professor of Industrial and Systems Engineering

## Abstract

An electric power system consists of three major components: generation, transmission and distribution. Electricity is usually generated in remote generation plants and carried through high voltage transmission lines to distribution substations. The distribution system delivers the electricity safely and reliably to the end customers. When the customers' demand increases, the transmission network has to be expanded to maintain the reliability of the network. In the first chapter of this dissertation, we propose a new method to compute the operational cost for the transmission network expansion. The proposed method is based on multivariate interpolation which reduces the computational time of the solving algorithm significantly. In the second chapter, we enhance the operational performance of the microgrids as part of the distribution grid. We introduce an efficient way to integrate a parking facility of electric vehicles (EVs) into the microgrids as a storage resource. By using the vehicle to grid technologies which enable the microgrid to withdraw energy from the batteries of the EVs, energy supply from the EVs' batteries can be a cost-efficient alternative. The ability to store and withdraw energy from the EVs allows the microgrid to shift energy purchases from high price to low price hours during the day. Finally, in the third chapter, we analyze the long term economics of EVs integration into the microgrids. We develop an investment model to determine the optimal capacity of the parking facility for EVs. Similar to the transmission network expansion, the required capital investment for the vehicle to grid technologies and the operational cost of the microgrid over the planning horizon are considered and minimized. We propose a new approach to minimize the total cost of investment and operation. Experimental results confirm that investing in the vehicle to grid technologies in the parking facility reduces the microgrid's cost of electricity supply in the long run.

## Acknowledgments

I would like to express the deepest appreciation to my PhD adviser, Dr. Jorge Valenzuela, for his endless support and persistent guidance. He continually mentored me through my graduate education and kept me engaged with my research. I truly enjoyed working under his supervision and expert direction.

I would like to acknowledge my committee members, Dr. Glenn Richey, Dr. Alexander Vinel and Dr. Fadel Megahed. Many thanks to Dr. Richey for helping me out with all my academic and professional questions and for his friendship. I should also express my gratitude to Dr. Vinel and Dr. Megahed for their continuous support and constructive feedback throughout the entire dissertation process.

Last but not least, I would like to thank my caring parents for their unconditional love and limitless support. I also would like to thank my sister for her every day encouragement and inspiration. Without the love and support of my family, I would not be able to complete this dissertation. I am so grateful for my family, and would like to proudly dedicate this dissertation to them.

## Table of Contents

Abstract . . . . .	ii
Acknowledgments . . . . .	iii
List of Figures . . . . .	vii
List of Tables . . . . .	ix
Introduction . . . . .	2
1 Transmission Expansion Planning Using Multivariate Interpolation . . . . .	3
1.1 Abstract . . . . .	3
1.2 Introduction . . . . .	4
1.3 Mathematical Model and Reliability Consideration . . . . .	7
1.3.1 Multiyear TEP Problem Formulation . . . . .	7
1.3.2 N-1 Security Criterion . . . . .	9
1.4 Multivariate Interpolation . . . . .	10
1.4.1 BPSO Algorithm . . . . .	11
1.4.2 Multivariate Interpolation . . . . .	13
1.5 Experimental Results . . . . .	17
1.5.1 Garver's 6-bus system . . . . .	19
1.5.2 The multivariate interpolation error . . . . .	22
1.5.3 Comparing the results of the proposed and traditional methods . . . . .	24
1.5.4 IEEE 24-bus test system . . . . .	25
1.5.5 Comparing the results of the proposed and traditional methods . . . . .	29
1.5.6 Expansion planning for real-world power systems . . . . .	29
1.6 Conclusion . . . . .	31
References . . . . .	32

2	Microgrid Energy Scheduling Using Storage from Electric Vehicles . . . . .	38
2.1	Abstract . . . . .	38
2.2	Introduction . . . . .	38
2.3	Problem Description . . . . .	42
2.3.1	Modeling Uncertainty . . . . .	42
2.3.2	Parking Facility . . . . .	43
2.4	Problem Formulation . . . . .	43
2.4.1	Objective Function . . . . .	43
2.4.2	Constraints . . . . .	44
2.5	Solving Algorithm . . . . .	46
2.6	Stochastic Modeling of the Energy Storage . . . . .	48
2.7	Microgrid Description . . . . .	51
2.7.1	Microgrid Topology . . . . .	51
2.7.2	EVs Parking Battery . . . . .	52
2.7.3	Day-ahead energy prices and power distributor . . . . .	53
2.7.4	Net Demand Uncertainty . . . . .	54
2.8	Simulation Results . . . . .	55
2.8.1	Effect of using the parking facility . . . . .	56
2.8.2	The value of considering uncertainty . . . . .	57
2.8.3	Effect of battery wear cost . . . . .	58
2.8.4	Effect of the EVs parking time on expected cost savings . . . . .	58
2.8.5	Effect of arrival and departure rates . . . . .	59
2.8.6	Effect of market price fluctuations . . . . .	59
2.8.7	Interaction effect of market price fluctuations and EVs' arrival and departure rates . . . . .	60
2.8.8	Effect of restricting the departures . . . . .	62
2.9	Conclusions . . . . .	62

References . . . . .	64
3 Optimal Investment to Upgrade a Microgrid Parking Facility with V2G Technology	68
3.1 Abstract . . . . .	68
3.2 Introduction . . . . .	68
3.3 Problem Description . . . . .	70
3.3.1 Parking facility for energy storage . . . . .	71
3.3.2 Modeling Uncertainty . . . . .	71
3.4 Problem Formulation . . . . .	71
3.4.1 Objective Function . . . . .	72
3.4.2 Constraints . . . . .	72
3.5 Solving Algorithm . . . . .	72
3.5.1 Finding the optimal value of $n$ . . . . .	73
3.5.2 Computing the operation cost . . . . .	73
3.6 Stochastic modeling of the parking facility . . . . .	75
3.7 Microgrid Description . . . . .	75
3.7.1 Microgrid Topology . . . . .	75
3.7.2 EVs Parking Battery . . . . .	75
3.7.3 Day-ahead energy prices and power distributor . . . . .	76
3.7.4 Net Demand Uncertainty . . . . .	78
3.8 Simulation Results . . . . .	78
3.8.1 Effect of the V2G technology . . . . .	81
3.8.2 Payback Period . . . . .	81
3.8.3 Effect of uncertainty . . . . .	81
3.9 Conclusions . . . . .	82
References . . . . .	84

## List of Figures

1.1	Multivariate interpolation on a function of two variables . . . . .	14
1.2	The flowchart of the solving algorithm . . . . .	18
1.3	Garver’s 6-bus test system . . . . .	19
1.4	The hourly demand for the first 100 hours of the first year . . . . .	20
1.5	Oil price for the first 50 days of the first year . . . . .	21
1.6	Natural gas price for the first 50 days of the first year . . . . .	21
1.7	The multivariate interpolation for the described 6-bus test system . . . . .	22
1.8	MAE for different number of breakpoints . . . . .	23
1.9	The computed operation cost difference between the trilinear interpolation and the OPF problem for the first 100 hours of year one . . . . .	24
1.10	IEEE 24 bus test system . . . . .	27
2.1	Software interaction to solve the Benders’ decomposition . . . . .	47
2.2	The solving algorithm’s flow chart . . . . .	49
2.3	14-bus microgrid test system . . . . .	51
2.4	The scenario sample for the number of parked EVs. . . . .	53

2.5	Energy price in the day-ahead. . . . .	53
2.6	Sample of net load scenarios . . . . .	54
2.7	The effect of parking time on the expected cost savings . . . . .	59
3.1	Nelder-Mead algorithm . . . . .	74
3.2	One scenario for the available EVs in the parking during a week in spring . . . .	77
3.3	Energy price in the day-ahead during a week in spring . . . . .	77
3.4	Three of the net demand scenario for one week from the spring season of year one	79
3.5	The convergence of the Nelder-Mead algorithm . . . . .	80
3.6	Discounted payback period considering investment on 320 V2G stations . . . . .	82

## List of Tables

1.1	Interpolated value of Y function at point E (1.8,2.7) . . . . .	15
1.2	The peak demand data for each year of the 10-year horizon period . . . . .	17
1.3	Data for annual average price of the oil and natural gas . . . . .	17
1.4	Data associated to the parallel elements in each line . . . . .	23
1.5	Added lines to the Garver’s network based on the proposed and traditional methods	26
1.6	The annual operation and investment costs for the Garver’s network . . . . .	26
1.7	Data associated to the parallel elements for 24 bus system . . . . .	28
1.8	Annual average fuel price . . . . .	28
1.9	The peak demand data for each year of the 10-year horizon period . . . . .	28
1.10	Added lines to the 24 bus network based on the proposed and traditional methods	30
1.11	The annual operation and investment costs for IEEE 24 bus system . . . . .	30
2.1	Unit commitment technical data . . . . .	52
2.2	Purchases/sales in the day ahead . . . . .	55
2.3	Charging/discharging of the parking battery . . . . .	56
2.4	Purchases/sales in the day ahead . . . . .	56
2.5	Purchases/sales in the day ahead . . . . .	57
2.6	Effect of battery wear cost . . . . .	58
2.7	Arrival Rates ( $\lambda$ ) for different cases at each hour . . . . .	60
2.8	Microgrid’s cost savings under different fluctuation rates . . . . .	60
2.9	Hypothetical patterns for day ahead market prices (\$/MWh) . . . . .	61

2.10 Cost savings under different price profiles and arrivals/departures. . . . . 62

3.1 Arrival and departure rates for a week in spring . . . . . 76

3.2 Investment and operation costs for 320 V2G . . . . . 79

3.3 Investment and operation costs for 100 V2G . . . . . 80

3.4 Investment and operation costs for 500 V2G . . . . . 80

## Introduction

In an electric power system, the transmission network transfers electricity at high voltages from the power plants to the distribution substations. The distribution system lowers the voltage from the transmission network and delivers the electricity safely to the end customers.

When the customers' demand grows, the transmission network needs to be expanded to meet the customers' new demand and maintain the reliability of the power delivery. The transmission network expansion can involve reinforcing new transmission lines and adding new sources of energy to the transmission network. Investment needs for the expansion of the transmission network can be significant and depend on the length of the planning horizon, network topology and the future demand. In addition to capital investment costs, operational costs must also be taken into account. Operational costs include the costs of generation and maintenance. As the computation of the operation cost for each hour over a long planning horizon can be very time-consuming, in the first chapter of this dissertation, we introduce a new method to accelerate the computations.

The energy distribution system is undergoing a major transformation from a simple low-voltage power delivery system to a grid modernization tool. Integration of distributed generators (DGs) and renewable energy resources into the distribution system and emergence of microgrid technologies have revolutionized the power delivery system. Microgrids are considered as small-scale versions of the current bulk power system that can operate in grid-connected and autonomous modes. The adoption of microgrids as smart distribution systems is growing and the recent wave of announced projects are enabling further developments. Microgrids integrate the local renewable resources, interact with power markets, provide local load control and allow the system to efficiently store energy in small scales.

Due to the intermittency of the renewable resources and the market price fluctuations, energy storage can play an important role in the energy scheduling of microgrids. The ability to store energy allows the microgrid to be more flexible in interacting with the energy markets. However, investment needs for energy storage technologies are high and the provided capacities are not significant. One of the energy storage resources that recently has received a substantial attention from the research community is the batteries of the electric vehicles (EVs). Since a typical EV is parked an average of 95% of the time, its battery can be used as an energy storage device for the grid. By using the vehicle to grid (V2G) technologies which enable the system to withdraw energy from the batteries of the EVs, energy supply from the EVs' batteries to the grid can be a cost-efficient alternative. Especially, when the number of EVs participating in the V2G program becomes considerable, the provided capacity for the storage and the withdrawn energy from the vehicles can reach significant quantities. Another contribution of this dissertation is to introduce an efficient way to integrate the parking facilities of the EVs into the microgrids as a storage resource and analyze the long term economics of this integration. Similar to the transmission network expansion, to make economic decisions in a long planning horizon for integrating the EVs parking facilities into the microgrids, the required capital investment for the V2G equipment and the operational cost of the microgrid over the planning horizon are considered and minimized. This dissertation outlines a plan of research that will consider the operational and investment solutions for the transmission expansion and distribution system upgrade in the electrical grid.

The remainder of this dissertation is organized as follows. Chapter 1 describes the transmission expansion planning problem and introduces the multivariate interpolation to accelerate the operation cost computations. Chapter 2 proposes a new model for integration of an EV parking facility with uncertain storage capacity into the microgrid. Finally, Chapter 3 discusses the long term economics of integration of an EV parking facility into the microgrid and determines the optimal investment on the V2G technology in the parking facility by minimizing the total costs.

## Chapter 1

### Transmission Expansion Planning Using Multivariate Interpolation

#### 1.1 Abstract

The total cost of the Transmission Expansion Planning (TEP) problem consists of investment and operation costs. The former is the required capital investment cost for new circuits throughout the network, and the latter is the cost of optimal generation dispatch to meet the demand at each hour. Traditionally, due to computational limits and long-term planning, the operation cost is not computed for hourly demand in the TEP problem. It is typically computed for the peak demand occurring during each year. In addition, the price of fuel used in the operation problem is considered fixed rather than variable over time. In this chapter, we use a multivariate interpolation method to compute the operation cost for the TEP problem in which the demand changes from hour to hour and the fuel price from day to day. A binary particle swarm optimization (BPSO) is proposed to solve the TEP problem. We apply our method to the Garver's 6-bus system and the IEEE 24-bus system for a planning horizon of ten years. By using the multivariate interpolation, the computational time of the solving algorithm is reduced. We compare our method with traditional methods based on the total cost of the obtained expansion plans. Experimental results show that the proposed method is an enhancement to solving the multi-year security-constrained TEP problem.

**Keywords:** Transmission Expansion Planning, Multivariate interpolation, Binary particle swarm optimization

## 1.2 Introduction

The TEP problem determines where, how many, and when new circuits should be installed to reinforce the existing transmission network. In order to solve the TEP problem, we can break it down into two sub-problems: the investment problem and the operation problem. The former minimizes the capital investment cost required for new circuits over the planning horizon. The latter, the OPF problem, determines the optimal output of the generating units to meet the demand, where a certain set of operational and transmission constraints are imposed. The solution of the OPF problem depends on the values of several parameters, particularly time-varying parameters, such as demand and fuel price. Changing the values of the parameters will change the solution of the OPF problem. As the demand alters from hour to hour, the OPF problem has to be solved for hourly demand to obtain the operation cost of the system. However in the TEP, the OPF problem is solved only for a limited number of demands rather than the hourly demand over a year. That is, the computed operation cost for those few demands multiplied by the number of hours in the year is used to approximate the annual operation cost. In the literature, solving the TEP problem using the annual peak demand is very common[1, 2, 7, 4]. Lately, in addition to the peak demand, the operation cost for a few other demands is also computed. For instance, Hinojosa et al. [5] divided the year into three unequal intervals and computed the operation cost based on three different demands: valley, mean, and peak for any one interval. Similarly, Aguado et al. [6] divided the year into four intervals and computed the operation cost for four different demands: low, medium-low, medium-high, and high within different intervals. However, considering even three or four different demands in year to compute the operation cost can hardly reflect the reality of the operations in a power system. Uncertainty in the electricity demand for the TEP problem has also been considered in the recent literature. Ref. [7] have used scenario planning to model the uncertainty of the system parameters. However, they only considered the peak demand to generate the scenarios related to the

electricity demand in the TEP problem. A comprehensive review of the recent published articles in the TEP area has been presented by Hemmati et al.[8].

As noted, the price of fuel is another changing parameter in the OPF problem that should be considered. For the fossil-fuel power plants, fuel cost is the main driver of the operation cost. The market price of some fuel is highly volatile. For instance, the natural gas and oil market prices change on a daily basis. Most utility companies, in order to stabilize the price of the required fuel for power plants, make long term fuel contracts. Therefore, the cost of fuel in the power plants remains stable. However, the market value of the fuel they use does change from day to day. Hence, using the daily market value of the fuel in the OPF problem is essential to obtain a more accurate value for the operation cost. Despite the fact that the fuel prices change over time, they are usually assumed fixed over the planning horizon. For instance, Sepasian et al.[9] presented a multiyear hybrid generation/transmission expansion problem including the fuel supply cost. They considered a fixed fuel price in the model during the planning years. Sharan et al.[10] considered the fuel cost, fuel transportation cost, and also the fuel constraints in the model. Similarly, the fuel price was assumed to be fixed within the planning horizon.

Our primary goal is to show that computing the operation cost based on peak demand and average fuel price is not accurate and may result in more costly expansion plans for the TEP problem. Therefore, we improve accuracy by considering the hourly demand instead of annual peak demand and daily fuel prices instead of annual average fuel price. As the fuel price does not change during a day, we model it on a daily basis.

In order to compute the hourly operation cost, the OPF problem has to be solved at each hour. However, solving the OPF problem for each hour over a long planning horizon can be extremely time-consuming. At the first attempt to overcome this issue, we may employ the post-optimality analysis of the problem. Post-optimality analysis of an optimization problem determines the optimal solution after changing the parameters without having to

resolve the problem. As the OPF problem is a linear programming (LP) problem, post-optimality analysis of an LP problem should be considered. For the LP problems, the effect of single and simultaneous variation in the right hand side and the cost coefficients vectors on the problem's optimal solution have been widely studied [11, 12]. Greenberg [13] established theorems about the simultaneous variation of the parameters when the primal and dual are in canonical form. However, his analysis was based on the assumption that the variation occurs in a single direction. Making the same assumption for the OPF problem does not sound reasonable as the demand and fuel price can change in random directions. Therefore, rather than using the post-optimality analysis, we directly quantify the operation cost value by multivariate interpolation.

To solve the TEP problem, different mathematical and Meta-heuristic methods have been proposed. Several mathematical methods such as linear programming[14, 15, 16], dynamic programming [17], nonlinear programming [18], and mixed integer programming [19] have been used to obtain the optimal solution for the TEP problem. Optimization techniques such as Benders [20, 21] and hierarchical [22] decompositions have also been utilized. Recently, the Meta-heuristic methods have received considerable attention. The TEP problem has been solved using genetic algorithms (GAs) [23, 4] , game theory[24], evolutionary algorithms [25], fuzzy approach [26], simulated annealing (SA) [22], particle swarm optimization (PSO)[25, 7], evolutionary particle swarm optimization (EPSO)[27], discrete evolutionary particle swarm optimization (DEPSO) [28] and ant colony optimization [25].

We use BPSO, a binary version of the PSO algorithm, to solve the TEP problem. The BPSO is easy to code and it has been shown to be efficient for solving discrete optimization problems. Shayeghi et al. [29] used a non-binary discrete PSO, Fuerte-Ledezma et al. [30] a BPSO and Kimiyaghalam et al.[31] an improved BPSO to solve the TEP problem. Kimiyaghalam et al. claimed that their proposed version converges faster than a basic BPSO. As the main contribution of our work is using the multivariate interpolation to compute the hourly operation cost, we code a standard version of the BPSO algorithm.

### 1.3 Mathematical Model and Reliability Consideration

#### 1.3.1 Multiyear TEP Problem Formulation

The objective of the TEP problem is to identify the best set of circuits to be added over the planning horizon. The total cost of the power system is minimized while a specific set of constraints are imposed to the system. In the TEP problem, a DC lossless model is usually used based on the assumption that the line losses are negligible. However, ignoring the line losses over a long planning horizon may result in a different network expansion plan [2]. Therefore, we considered line losses in modeling the TEP problem. The transmission line losses for a DC power flow system can be approximated with the expression (1.1)

$$Pf_p^{Loss(i,j)} \approx 2G_{ij}(1 - \cos(\theta_i - \theta_j)) = 4G_{ij}(\sin^2(\theta_i - \theta_j)/2) \approx G_{ij}(\theta_i - \theta_j)^2 \quad (1.1)$$

A quadratic relationship between the line losses and voltage angle differences can be problematic in terms of convergence properties and finding the exact optimal solution of the OPF problem. Therefore, a linear model for line losses should be considered. Several methods have been proposed to represent a linear model for the line losses in the TEP problem [32, 33, 2]. One approach is to approximate  $(\theta_i - \theta_j)^2$  using piecewise linear functions and the other is to approximate  $(Pf_p^{i,j})^2$ . Due to several advantages explained in [2] we use the approach proposed by Zhang et al. in which the losses are represented as piecewise linear functions of the line flows instead of the voltage angle differences. The relationship between  $Pf_p^{Loss(i,j)}$  and  $(Pf_p^{i,j})^2$  can be expressed by equation (1.2):

$$Pf_p^{Loss(i,j)} = (G_{i,j}/\gamma^2)(Pf_p^{i,j})^2 \quad (1.2)$$

The piecewise linear model associated to the  $(Pf_p^{i,j})^2$  has been expressed by (1.6)-(1.11), where  $(Pf_p^{i,j})^2$  is approximated by  $L$  linear sections.  $(Pf_p^{i,j})^+$  and  $(Pf_p^{i,j})^-$  are two non-negative variables to represent the power flow between buses  $i$  and  $j$ .

The formulation of the TEP problem is indicated by Equations (1.3)-(1.16). The objective function of the model, given in (1.3), corresponds to the sum of the operation cost of the power system and the investment cost of the newly added circuits to the transmission network. The operation cost at each period is the product of the amount of fuel used in each generator by the per unit price of the fuel.

$$Min z = \sum_{p=1}^P \left( \frac{UF_{f,p}(MF_{p,k}^{f,i}) + \sum_{n=1}^N K_p^n (IC_p^n)}{(1+r)^p} \right) \quad (1.3)$$

Subject to:

$$M_p(Pf_P^{i,j}) + PG_{p,k}^i + PGV_p^i = D_p^i + Pf_P^{Loss(i,j)} \quad (1.4)$$

$$Pf_P^{i,j} - \gamma_{i,j}(n_{i,j}^0 + n_{i,j})(\theta_i - \theta_j) = 0 \quad (1.5)$$

$$Pf_P^{i,j} = (Pf_P^{i,j})^+ - (Pf_P^{i,j})^- \quad (1.6)$$

$$|Pf_P^{i,j}| = \sum_{l=1}^L \Delta Pf_P^{i,j}(l) = (Pf_P^{i,j})^+ + (Pf_P^{i,j})^- \quad (1.7)$$

$$0 \leq \Delta Pf_P^{i,j}(l) \leq (n_{i,j}^0 + n_{i,j}) \overline{(Pf_P^{i,j})} / L \quad (1.8)$$

$$Pf_P^{Loss(i,j)} = (G_{i,j} / \gamma^2) \sum_{l=1}^L k_l (\Delta Pf_P^{i,j}(l)) \quad (1.9)$$

$$k_l = (2l - 1) \overline{(Pf_P^{i,j})} / L \quad (1.10)$$

$$|Pf_P^{i,j} + Pf_P^{Loss(i,j)}| \leq (n_{i,j}^0 + n_{i,j}) \overline{(Pf_P^{i,j})} \quad (1.11)$$

$$MF_{p,k}^{f,i} \cdot HHV_f = PG_{p,k}^i \cdot Nh_{k,f} \cdot HR_k^i \quad (1.12)$$

$$|Pf_P^{i,j}| \leq (n_{i,j}^0 + n_{i,j}) \overline{(Pf_P^{i,j})} \quad (1.13)$$

$$0 \leq PG_{p,k}^i \leq \overline{PG_{p,k}^i} \quad (1.14)$$

$$0 \leq PGV_{p,k}^i \leq D_p^i \quad (1.15)$$

$$0 \leq n_{i,j} \leq \overline{n_{i,j}} \quad (1.16)$$

Constraints in (1.4) represent the power balance at bus  $i$ . Constraints in (1.5) represent the power flow on each line. Constraints (1.6) to (1.10) are to ensure that  $\Delta P f_P^{i,j}(l)$  with smaller values will be chosen to fill first. Constraints in (1.11) represent the thermal flow limits over transmission lines. Constraints in (1.12) represent the relationship between the consumed fuel in the power station and the generated power [34]. Constraints in (1.13) guarantee the power flow at each line do not exceed the maximum allowed level. Constraints in (1.14) represent the generating units operating capacity and constraints in (1.15) and (1.16) indicate the fictitious generation limit and the maximum allowed number of circuits from bus  $i$  to bus  $j$ , respectively.

### 1.3.2 N-1 Security Criterion

A secure power system must be able to tolerate the outage of any component and continue to deliver electric power safely and reliably. When a power system withstands the outage of a single component out of  $N$  components, it is said to be N-1 secure. The N-1 secure system means that failure of any one line in the transmission system does not cause overloading in the other lines. Likewise, the integrity of the system after the failure should be maintained. The N-1 security is fundamental to the network's expansion, and it must be achieved regardless of the imposed cost [35]. In order to meet the N-1 security criterion in the TEP problem, the total number of different states at which a contingency may occur should be computed. Afterwards, the system condition should be analyzed once a contingency occurs. The number of contingencies to be considered in a transmission system is  $N_L+1$  (single line outage plus no outage), where  $N_L$  is the number of lines in the system. Therefore, the total number of states for the N-1 security analysis for a planning horizon of  $N_Y$  years and  $N_D$  demand is  $N_Y \times N_D \times N_L+1$ . Clearly, evaluating a complete N-1 security analysis for all states in a system is very time consuming and usually unnecessary. Therefore, in order to decrease the computational time of the analysis, we evaluate the N-1 criterion only for the annual peak demand. As a system can tolerate a line outage for the

peak demand, it will most likely be able to tolerate lower demands [36]. To evaluate the N-1 security criterion, we add a virtual generator to each bus of the N-1 system and set a very high cost for their output to penalize the objective function of the OPF problem. After solving the OPF for N-1 system, if the output of a virtual generator is greater than zero, the system needs additional generation to meet the demand, that is, the transmission system is not N-1 secure. We have summarized the required steps to analyze the N-1 security criterion in the methodology section.

#### 1.4 Multivariate Interpolation

As noted earlier, to compute the annual operation cost, rather than solving the OPF problem at each hour, we could employ the post-optimality analysis to obtain the optimal solution after the values of demand and fuel price change. However, when the variations exceed an allowable level, the post-optimality analysis will no longer be valid and has to be revised. Moreover, when multiple parameters are changed independently in different directions, it becomes considerably complicated. Therefore, rather than using the post-optimality analysis, we directly quantify the objective function value by multivariate interpolation. In comparison to the post-optimality analysis, the multivariate interpolation requires less sophistication, is much faster, and approximates the objective function value with a negligible error. Moreover, for the post-optimality analysis, when the number of changing parameters increases, it is almost impossible to exactly determine the transition points of the optimal basis. While using the interpolation, we do not have to pinpoint the transition points.

After we obtained the operation cost of all hours in a year by multivariate interpolation, The BPSO algorithm integrates the annual operation cost and investment cost of the newly added circuits to determine the optimal expansion plan over the planning horizon. The methodology used to solve the multiyear security constraint TEP problem is described in the following sections.

### 1.4.1 BPSO Algorithm

Originally introduced by Eberhart and Kennedy in 1995, the particle swarm algorithm adjusts the trajectories of a population of particles through a problem space on the basis of information about each particle's previous best performance and the best previous performance of its neighbors [37]. The PSO was originally developed for real-valued spaces. However, in many problems, discrete valued variables are widely utilized [38]. We describe the BPSO algorithm used to solve the TEP problem through the following procedure:

#### a) *Representing candidate expansion plans*

In the BPSO algorithm, a candidate expansion plan is represented by a particle's position vector  $P_k$ , which is defined by (1.17):

$$P_k = (P_{k,1}, P_{k,2}, P_{k,3}, \dots, P_{k,N}) \quad (1.17)$$

Where  $N$  is the total number of candidate lines for a particular network topology and  $k$  is the iteration number. For instance, if four circuits are allowed between two buses, the position vector contains  $4 \times \binom{n}{2}$  components for a transmission system with  $n$  buses. This vector for a problem that has been modeled for ten years will be a matrix of 10 by  $4 \times \binom{n}{2}$ . Each particle's velocity vector at iteration  $k$  is given by (1.18):

$$V_k = (V_{k,1}, V_{k,2}, V_{k,3}, \dots, V_{k,N}) \quad (1.18)$$

The best visited position (personal best) for a particle is defined by (1.19):

$$P_{P.best,k} = (P_{P.best,k1}, P_{P.best,k2}, P_{P.best,k3}, \dots, P_{P.best,kN}) \quad (1.19)$$

And the best position explored so far (global best) is denoted by (1.20):

$$P_{global,k} = (P_{global,k1}, P_{global,k2}, P_{global,k3}, \dots, P_{global,kN}) \quad (1.20)$$

b) *Updating the particle's velocity and position*

The particle's velocity vector is updated according to (1.21):

$$V_k = \Psi V_k + c_1 r_1 (p_{P.best,k} - p_k) + c_2 r_2 (p_{P.global,k} - p_k) \quad (1.21)$$

Where acceleration coefficients  $c_1$  and  $c_2$  are positive constants named cognitive and social parameters, respectively,  $r_1$  and  $r_2$  represent independent random numbers which are uniformly distributed in the range  $[0,1]$ , and  $\Psi$  is the inertia weight factor that controls the amount of the previous velocity of the particle to be maintained in the current cycle [39].

In the BPSO, the personal best and global best of the particles are updated as in real-valued version. However, the major difference between BPSO and real-valued PSO is that the velocities of the particles are restricted within the range  $[0,1]$ . As in [38], we map the real-valued velocity numbers to the range  $[0,1]$ , using the sigmoid function given by (1.22):

$$V_k = \frac{1}{1 + e^{-V_k}} \quad (1.22)$$

The particle's position vector is updated according to (1.23):

$$P_k = \begin{cases} 1 & \text{if } r_k \leq \frac{1}{1+e^{-V_k}} \\ 0 & \text{otherwise} \end{cases} \quad (1.23)$$

Where  $r_k$  is a uniform random number in the range  $[0,1]$ .

c) *Computing the fitness functions*

The fitness function of a particle's position  $P_k$  is the total costs over the planning horizon (P periods) that is calculated by (1.24):

$$F_P = \sum_{p=1}^P \left( \frac{O(P_k) + \sum_{n=1}^N (IC_p^n \times P_k)}{(1+r)^p} \right) + M \times Rel \quad (1.24)$$

Where  $M$  is a huge penalty cost and  $Rel$  is a binary variable that equals to one if the system does not meet the N-1 security criterion. The value of  $O(P_k)$  is the operation cost of the candidate plan  $P_k$ . In our comparison study, the value of  $O(P_k)$  is computed as indicated in (1.25):

$$O(P_k) = \begin{cases} Y(P_k) & \text{Multivariate interpolation solved for hourly demand} \\ OPF(P_k) & \text{OPF problem solved for the annual peak demand} \end{cases} \quad (1.25)$$

#### 1.4.2 Multivariate Interpolation

In this section, we describe the multivariate interpolation method to compute the hourly operation cost which is used to calculate the fitness function as indicated in (1.24). The first step of the method is to determine the changing parameters of the OPF problem. We assume that the demand and fuel prices (the right-hand-side and cost coefficients) are the changing parameters. The second step is to determine the range of the changing parameters, the minimum and maximum values. The range is then broken at points (breakpoints) uniformly distributed over the range. The OPF problem is solved for all combinations of breakpoints of the demand and fuel prices. The operation cost of a combination of demand and fuel prices not included by the breakpoints is estimated by the following multivariate interpolation method.

Interpolation on a function of more than one variable is called multivariate interpolation. Whenever the linear standard algebra method is employed to find the value of the function at an arbitrary point, the multivariate interpolation is called multi-linear. The multi-linear interpolation methods can approximate the value of an arbitrary point inside a right rectangular polytope using the data of the vertex points [40]:

We first explain the multivariate interpolation method using the bilinear case, the changing of two parameters. Then, we provide general equations for the multivariate case. Assume we have a function  $y=f(x_1,x_2)$  and four points:  $((x_{11},x_{21}),\dots,(x_{12},x_{22}))$  that are the vertices of the rectangle ABCD shown in Figure 1.1. Assume the value of the function  $y$  is known at the four points and they are denoted by  $y_1, y_2, y_3,$  and  $y_4,$  respectively. An arbitrary point  $E$  located at  $(x_1,x_2)$  inside the rectangle divides the rectangle into four different partitions. To compute the  $y$ -value at the point  $E$ , we compute using (1.26) - (1.29) the normalized areas  $A_1, A_2, A_3,$  and  $A_4$  for each partition.

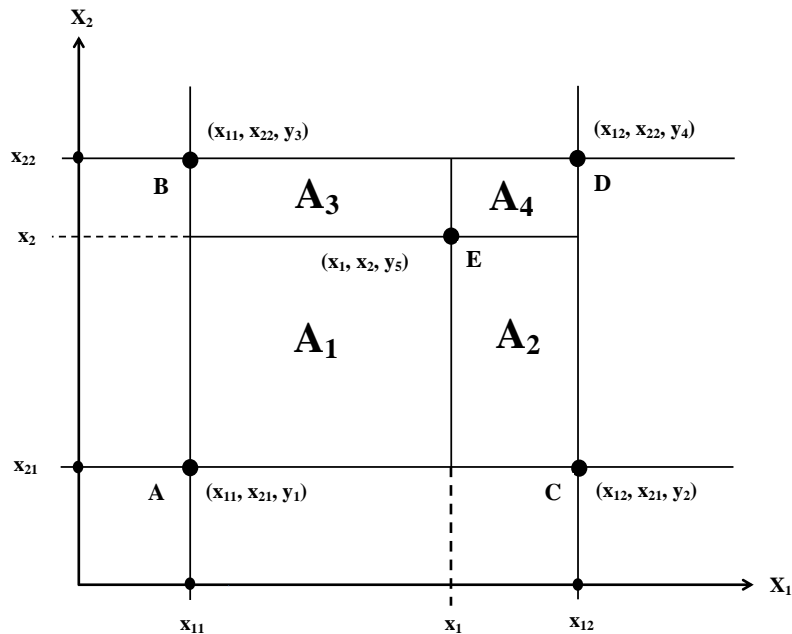


**Figure 1.1:** Multivariate interpolation on a function of two variables

$$A_1 = \left( \frac{(x_1 - x_{11})(x_2 - x_{21})}{(x_{12} - x_{11})(x_{22} - x_{21})} \right) \quad (1.26)$$

$$A_2 = \left( \frac{(x_{12} - x_1)(x_2 - x_{21})}{(x_{12} - x_{11})(x_{22} - x_{21})} \right) \quad (1.27)$$

$$A_3 = \left( \frac{(x_1 - x_{11})(x_{22} - x_2)}{(x_{12} - x_{11})(x_{22} - x_{21})} \right) \quad (1.28)$$

$$A_4 = \left( \frac{(x_{12} - x_1)(x_{22} - x_2)}{(x_{12} - x_{11})(x_{22} - x_{21})} \right) \quad (1.29)$$

The  $y$ -value of  $E$ ,  $y_5$ , is given by (1.30):

$$y_5 = y_1.A_4 + y_2.A_3 + y_3.A_2 + y_4.A_1 \quad (1.30)$$

In Table 1.1, we show the interpolation method for two arbitrary functions. Clearly, the interpolation error for the linear function is zero and for the nonlinear function is greater than zero.

**Table 1.1:** Interpolated value of Y function at point E (1.8,2.7)

Y=1.58X <sub>1</sub> +0.76X <sub>2</sub>						
Index number	Vertex	Y value	A <sub>i</sub>	Interpolated value	Function value	Error percentage
1	(1,2)	3.1	0.56			
2	(1,3)	3.86	0.24	4.896	4.896	0.00
3	(2,2)	4.68	0.14			
4	(2,3)	5.44	0.06			
Y=2.87X <sub>1</sub> <sup>2</sup> +1.42X <sub>2</sub> <sup>2</sup>						
Index number	Vertex	Y value	A <sub>i</sub>	Interpolated value	Function value	Error percentage
1	(1,2)	8.55	0.56			
2	(1,3)	15.65	0.24	20.41	19.65	3.85
3	(2,2)	17.16	0.14			
4	(2,3)	24.26	0.06			

To present the multivariate interpolation in a generic format, assume we have a function  $y = f(x_1, x_2, x_3, \dots, x_n)$  and  $2^n$  points that are the vertices of a right rectangular polytope. If an arbitrary point  $Z$  (given at  $z_1, z_2, \dots, z_n$ ) in the interior of the polytope is chosen, the

polytope is divided into  $2^n$  partitions. The  $y$ -value of  $Z$  can be computed by (1.31) - (1.35) [40]:

$$A_1 = \left( \frac{(z_1 - x_{10})(z_2 - x_{20}) \dots (z_n - x_{n0})}{(x_{11} - x_{10})(x_{21} - x_{20}) \dots (x_{n1} - x_{n0})} \right) \quad (1.31)$$

$$A_2 = \left( \frac{(z_1 - x_{10})(z_2 - x_{20}) \dots (x_{n1} - z_n)}{(x_{11} - x_{10})(x_{21} - x_{20}) \dots (x_{n1} - x_{n0})} \right) \quad (1.32)$$

$$\vdots \quad (1.33)$$

$$A_{2^n} = \left( \frac{(x_{11} - z_1)(x_{21} - z_2) \dots (x_{n1} - z_n)}{(x_{11} - x_{10})(x_{21} - x_{20}) \dots (x_{n1} - x_{n0})} \right) \quad (1.34)$$

Where point  $(x_{10}, x_{20}, \dots, x_{n0})$  is the polytope vertex nearest the origin, and point  $(x_{11}, x_{21}, \dots, x_{n1})$  is the vertex farthest from the origin. To compute the  $y$ -value of  $Z$ , each  $A_i$  is multiplied by the  $y$ -value of the corresponding diagonally opposite vertex. The  $y$ -value for  $Z$ , can be computed by (1.35):

$$y_Z = y_1 \cdot A_{2^n} + y_2 \cdot A_{2^{n-1}} + \dots + y_{2^{n-1}} \cdot A_2 + y_{2^n} \cdot A_1 \quad (1.35)$$

The accuracy of the interpolation method is determined by the number of breakpoints. It is clear as the number of breakpoints increases the interpolation error decreases. However, a larger number of breakpoints would require greater computational time. Therefore, we calculate an acceptable number of breakpoints by using the maximum amount of time we have available to run the BPSO algorithm. The number of breakpoint,  $B$ , for  $C$  number of changing parameters, is given by (1.36):

$$B = \sqrt[C]{\left( \frac{T}{Y \times N \times P \times t} \right)} \quad (1.36)$$

Where  $t$  denotes the computational time of solving one OPF problem for a specific transmission network,  $N$  is the number of iterations of the BPSO with  $P$  particles,  $Y$  is the number of years,  $T$  is the maximum amount of time we have available to run the BPSO.

The flowchart of the proposed methodology which is used to solve the TEP problem and evaluate the N-1 security criterion is given in Figure 1.2.

## 1.5 Experimental Results

We ran our experiments on the Garver’s 6-bus and the IEEE 24-bus test systems. In order to solve the OPF problem for the considered test systems, we used the IBM ILOG CPLEX interactive optimizer with Concert technology in C++. Concert Technology is a set of libraries offering an API that includes modeling facilities to allow a programmer to embed CPLEX optimizers in C++ [20]. The experimental results obtained by the proposed method are compared to those of a traditional method. In the traditional method, the OPF problem is solved for the annual peak demand and annual average fuel price.

**Table 1.2:** The peak demand data for each year of the 10-year horizon period

<i>BUS#</i>	<i>Year</i> <sub>0</sub>	<i>Year</i> <sub>1</sub>	<i>Year</i> <sub>2</sub>	<i>Year</i> <sub>3</sub>	<i>Year</i> <sub>4</sub>	<i>Year</i> <sub>5</sub>	<i>Year</i> <sub>6</sub>	<i>Year</i> <sub>7</sub>	<i>Year</i> <sub>8</sub>	<i>Year</i> <sub>9</sub>	<i>Year</i> <sub>10</sub>
1	20	22.97	26.39	30.31	34.82	40.00	45.95	52.78	60.63	69.64	80.00
2	60	68.92	79.17	90.94	104.47	120.00	137.84	158.34	181.89	208.93	240.00
3	10	11.49	13.20	15.16	17.41	20.00	22.97	26.39	30.31	34.82	40.00
4	40	45.95	52.78	60.63	69.64	80.00	91.90	105.56	121.26	139.29	160.00
5	60	68.92	79.17	90.94	104.47	120.00	137.84	158.34	181.89	208.93	240.00
Total	190.00	218.25	250.71	287.99	330.81	380.00	436.51	501.41	575.97	661.62	760.00

**Table 1.3:** Data for annual average price of the oil and natural gas

Fuel type	<i>Year</i> <sub>0</sub>	<i>Year</i> <sub>1</sub>	<i>Year</i> <sub>2</sub>	<i>Year</i> <sub>3</sub>	<i>Year</i> <sub>4</sub>	<i>Year</i> <sub>5</sub>	<i>Year</i> <sub>6</sub>	<i>Year</i> <sub>7</sub>	<i>Year</i> <sub>8</sub>	<i>Year</i> <sub>9</sub>	<i>Year</i> <sub>10</sub>
Oil(\$/barrel)	20	22.97	26.39	30.31	34.82	40.00	45.95	52.78	60.63	69.64	80.00
Natural gas(\$/Mcf)	6	6.81	7.91	9.09	10.47	12	13.78	15.83	18.19	20.89	24

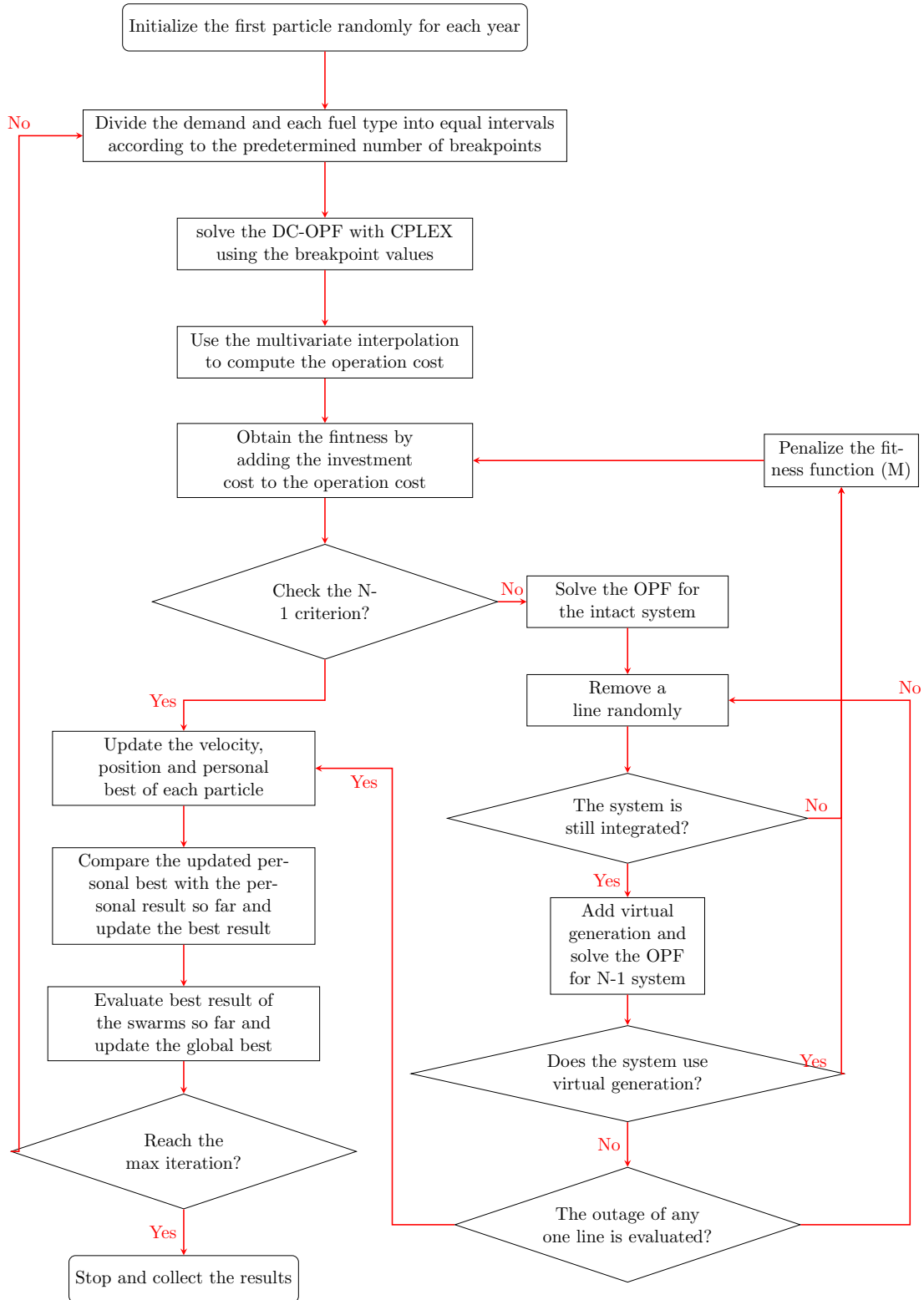


**Figure 1.2:** The flowchart of the solving algorithm

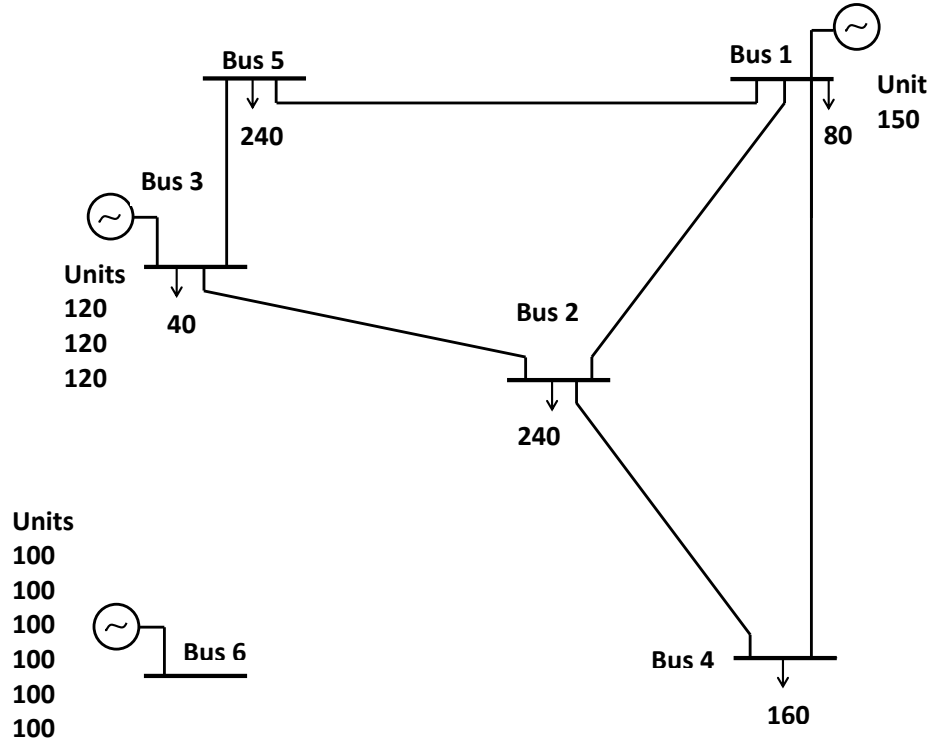


**Figure 1.3:** Garver's 6-bus test system

### 1.5.1 Garver's 6-bus system

The Garver's test system has been explained in [16] and its network is shown in Figure 1.3. We assume two types of fuel are being used in the power system. The active power stations, generators one to four, use oil to generate power for the current power demand. The power station six, which is going to enhance the power supply for the growing demand, is equipped with six natural gas generators. The peak demand data is given in Table 1.2 and the data for the annual average price of the oil and natural gas is given in Table 1.3. The increase rate of the demand is assumed to be 14.87% at each year. The hourly demand data used in the proposed method is generated based on the method explained in [42]. In [42], a typical year has been divided into three seasons, winter, summer and spring/fall. The hourly demand in a day during each season is presented in percent of the peak demand of the day

inside that season. We generate the hourly data based on the presented percentages and the annual growth rate. The hourly demand for the first 100 hours of the first year is shown in Figure 1.4. To generate the daily oil and natural gas prices for the proposed method, we collected the historical data for different fuel prices from [43]. We extracted the seasonal factor from the data and determined a typical pattern for the fuel price fluctuations during one year. Based on the determined pattern, we generated the daily fuel prices randomly for the first year. Then, we adjusted the generated fuel prices for a day according to the season it belongs to. For the following years, in addition to the described procedure, the annual growth rate was considered. The oil and natural gas prices for the first 50 days of the first year are shown in Figures 1.5 and 1.6, respectively. Since the prices of the two fuel types and the system demand are the changing parameters in the OPF problem, we use trilinear interpolation to estimate the hourly operation cost of the system.

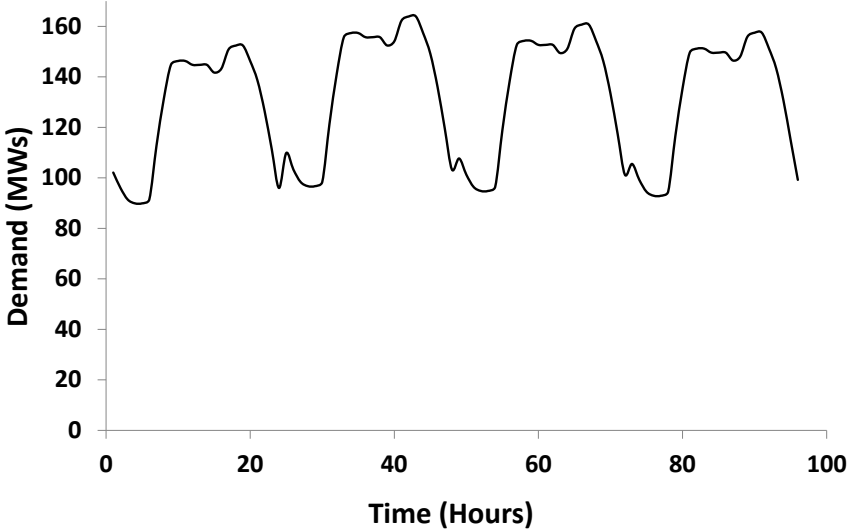


**Figure 1.4:** The hourly demand for the first 100 hours of the first year

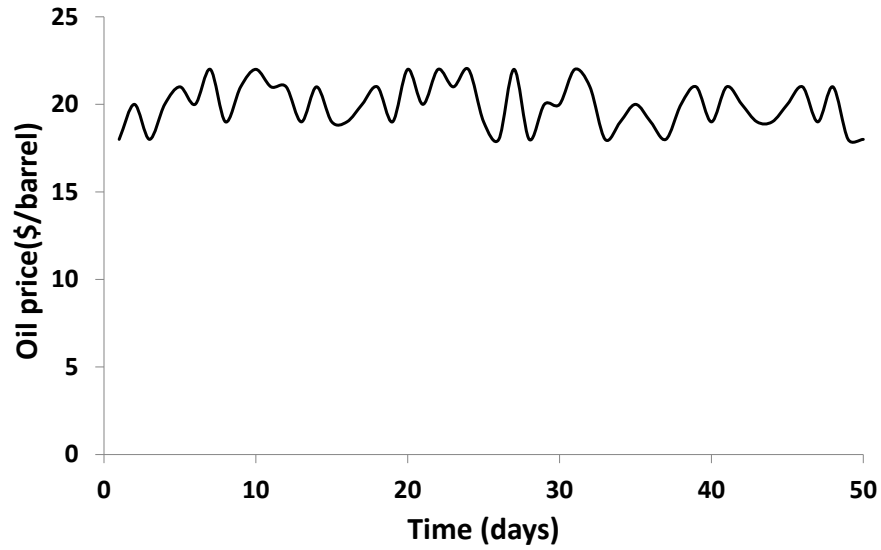


**Figure 1.5:** Oil price for the first 50 days of the first year

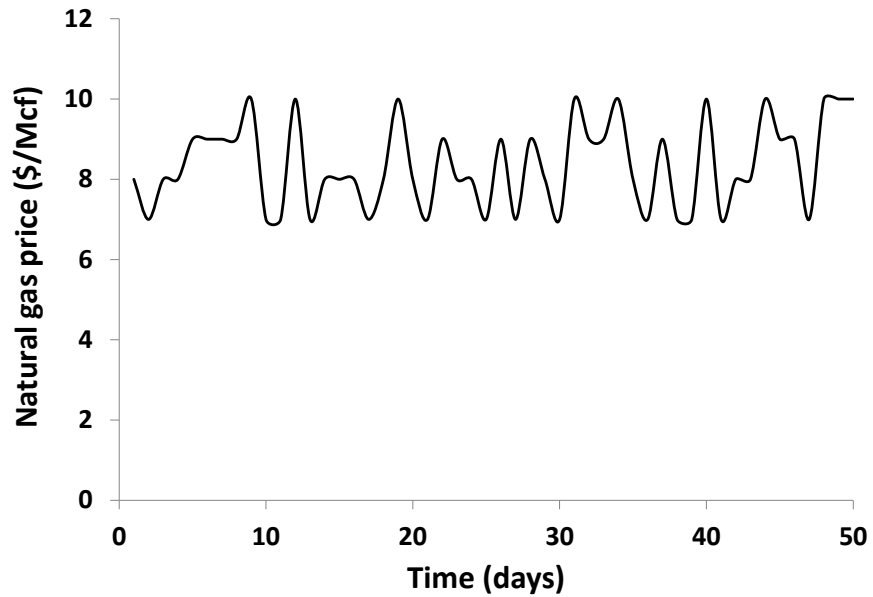


**Figure 1.6:** Natural gas price for the first 50 days of the first year

The trilinear interpolation is a method of linear interpolation on a function of three variables. It approximates the value of an arbitrary point inside the local axial rectangular prism using the data stored on the corners. To describe the trilinear interpolation, we create the interpolation for a candidate expansion plan for the Garver's 6-bus test system. We consider an expansion plan in which all of the buses in the network are connected to each

other and the maximum and minimum values of the demand, oil price and natural gas prices in one stage are [21,105], [14,70], [6,20], respectively. We divide each data range into five equal intervals and solve the OPF problem for all combinations of the breakpoints. Figure 1.7 shows the interpolation function for a fixed price of natural gas (10 \$/Mcf).

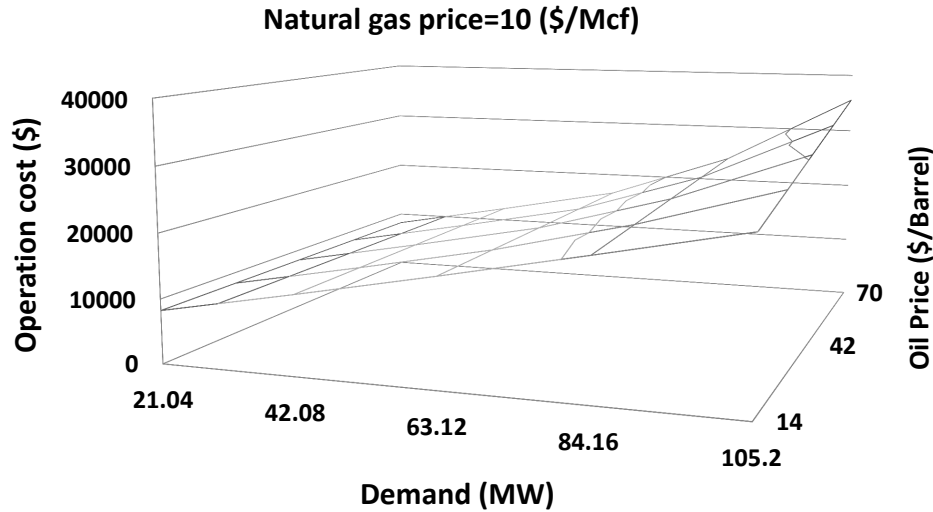


**Figure 1.7:** The multivariate interpolation for the described 6-bus test system

As noted earlier, the fitness function of the BPSO algorithm is the sum of the investment cost of the newly added circuits and the annual operation cost. Table 1.4 displays the data associated to the investment costs of the parallel circuits in each line. For the Garver’s network, we assumed the generator at bus 1, the three generators at bus 3 and the six generators at bus 6 have a maximum capacity of 150 MWs, 120 MWs, and 100 MWs, respectively. The maximum number of circuits between two buses is also considered to be four.

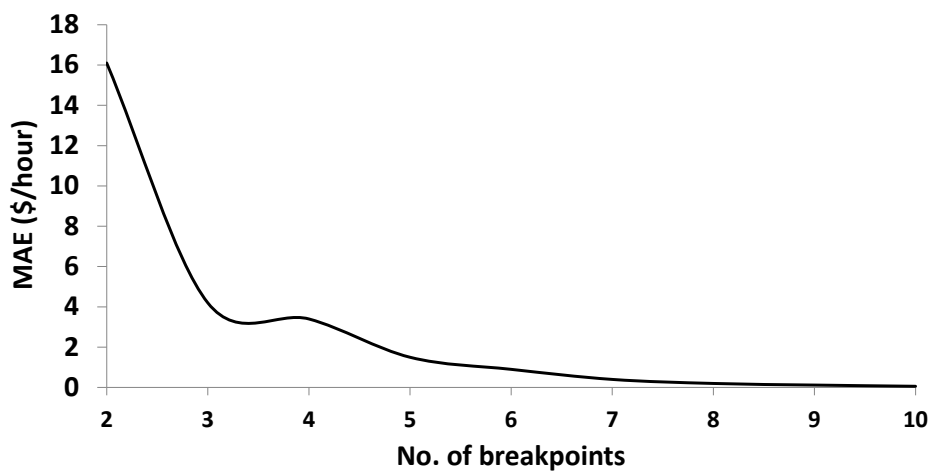
### 1.5.2 The multivariate interpolation error

To obtain the relative error between the interpolated value and the OPF optimal value, we take a random sample of 1000 points from each data range and compute the operation cost

**Table 1.4:** Data associated to the parallel elements in each line

No. of allowed elements	Line (from-to)	Length (miles)	R (p.u)	X (p.u)	Capacity (MW)	IC (M\$)
4	1-2	40	0.1	0.4	100	4
4	1-3	38	0.1	0.38	100	3.8
4	1-4	60	0.08	0.6	80	6
4	1-5	20	0.09	0.2	100	2
4	1-6	68	0.1	0.68	70	6.8
4	2-3	20	0.09	0.2	100	2
4	2-4	40	0.05	0.4	100	4
4	2-5	31	0.09	0.31	100	3.1
4	2-6	30	0.08	0.3	100	3
4	3-4	59	0.09	0.59	82	5.9
4	3-5	20	0.06	0.2	100	2
4	3-6	48	0.1	0.48	100	4.8
4	4-5	63	0.1	0.63	75	6.3
4	4-6	30	0.09	0.3	100	6.3
4	5-6	61	0.07	0.61	80	6.3

with the OPF problem and the trilinear interpolation for the selected points. Figure 1.8 shows the MAE of the sample for different number of breakpoints. As the number of breakpoints increases, the relative error between the interpolated value and the OPF optimal value is reduced.

**Figure 1.8:** MAE for different number of breakpoints

The difference between the computed operation cost by trilinear interpolation and the OPF problem for the first 100 hours of year one has been shown in Figure 1.9. The number of breakpoints is assumed to be 5. The error for the annual operation cost is 0.02%.

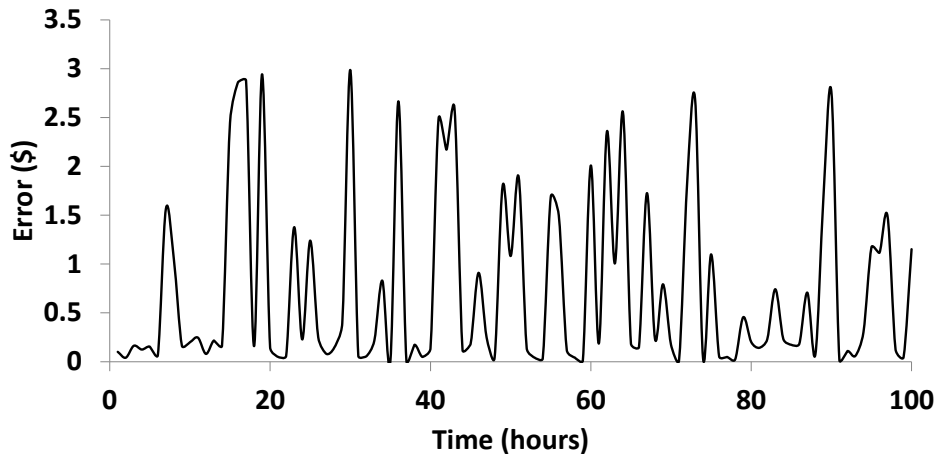


**Figure 1.9:** The computed operation cost difference between the trilinear interpolation and the OPF problem for the first 100 hours of year one

### 1.5.3 Comparing the results of the proposed and traditional methods

We ran the BPSO program for 100 iterations. In the BPSO algorithm,  $c_1$  was set at 1.5,  $c_2$  at 2.5, the inertia weight factor  $\Psi$  at 0.999 and the number of particles at 50. To determine the number of breakpoints for the trilinear interpolation, we set the maximum allowed computational time of the algorithm to 3 days. As it takes 0.04 seconds on average to solve the OPF problem for the Garver's 6-bus system, the number of breakpoints using (36) was computed to be 5. The algorithm's run time for the proposed method was 2 day and 18 hours and for the traditional method was 2 hours and 12 minutes on a 3 GHz Core 2 Due processor. In either method, after 80 iterations, no considerable change in the objective function value was observed. If we had used the OPF problem instead of multivariate

interpolation to compute the hourly operation cost in the BPSO, it would take 2 years and 8 days to compute the total operation cost for the BPSO. The number and the location of the newly added circuits are different in the obtained plans by the proposed and traditional methods. In the final plan obtained by the proposed and traditional methods, five and six new circuits, respectively, are added to the transmission network. The newly added circuits to the Garver’s 6-bus system based on both methods have been shown in Table 1.5. To compare the total cost of the two methods, we computed the hourly operation cost by solving the OPF problem at each hour for both plans. Table 1.6 summarizes the present worth of the annual operation and investment costs for the final plans. The total cost of the multivariate interpolation is \$3.8M less than the traditional plan.

#### **1.5.4 IEEE 24-bus test system**

The IEEE 24-bus test system has been explained in [42] and its network is shown in Figure 1.10. It contains 24 generation/load buses, 38 transmission lines and 33 generation units. The transmission line data is given in Table 1.7. We assume that three types of thermal generating plants, coal-fired, oil-fired, and natural gas-fired, are active in the system. The data for annual average fuel price is given in Table 1.8. Similar to the 6-bus system, we use the annual peak demand and average fuel price for the traditional method and hourly demand and daily fuel price for the proposed method to solve the TEP problem. To generate the demand and fuel price data, we use the same procedure explained in section 4.1. The increase rate of the demand is assumed to be 14.87% at each year. The peak demand data for each bus is also given in Table 1.9.

**Table 1.5:** Added lines to the Garver's network based on the proposed and traditional methods

Method	Line (from-to)	Year <sub>1</sub>	Year <sub>2</sub>	Year <sub>3</sub>	Year <sub>4</sub>	Year <sub>5</sub>	Year <sub>6</sub>	Year <sub>7</sub>	Year <sub>8</sub>	Year <sub>9</sub>	Year <sub>10</sub>	Total
Multivariate Interpolation	2-3		1									1
	2-6						1					1
	3-5	1										1
	4-6		1					1				2
OPF Problem	2-3		1									1
	2-5		1									1
	2-6								1			1
	3-5						1					1
	4-6				1					1		2

**Table 1.6:** The annual operation and investment costs for the Garver's network

Method	Demand	Fuel price	Cost type	Year <sub>1</sub>	Year <sub>2</sub>	Year <sub>3</sub>	Year <sub>4</sub>	Year <sub>5</sub>	Year <sub>6</sub>	Year <sub>7</sub>	Year <sub>8</sub>	Year <sub>9</sub>	Year <sub>10</sub>	Total
Multivariate Interpolation	Hourly	Daily price	Operation cost (\$10M)	2.2638	2.4632	2.6074	2.6989	2.8424	2.9380	3.0664	3.2089	3.5643	4.1050	29.758
			Investment cost	0.20	0	0	0.37566	0	0	0.16934	0.15395	0	0	0
			Total	2.4638	2.4632	2.6074	3.0746	2.8424	2.9380	3.2357	3.3629	3.5643	4.1050	30.657
OPF problem	Peak	Annual price	Operation cost(\$10M)	2.4619	2.4619	2.6060	2.6994	2.8429	2.9386	3.0678	3.2109	3.5666	4.1049	29.961
			Investment cost	0.51000	0	0	0	0	0.18628	0.11289	0	0.13995	0.12723	1.0764
			Total	2.9719	2.4619	2.6060	2.6994	2.8429	3.1249	3.1807	3.2109	3.7066	4.2321	31.037

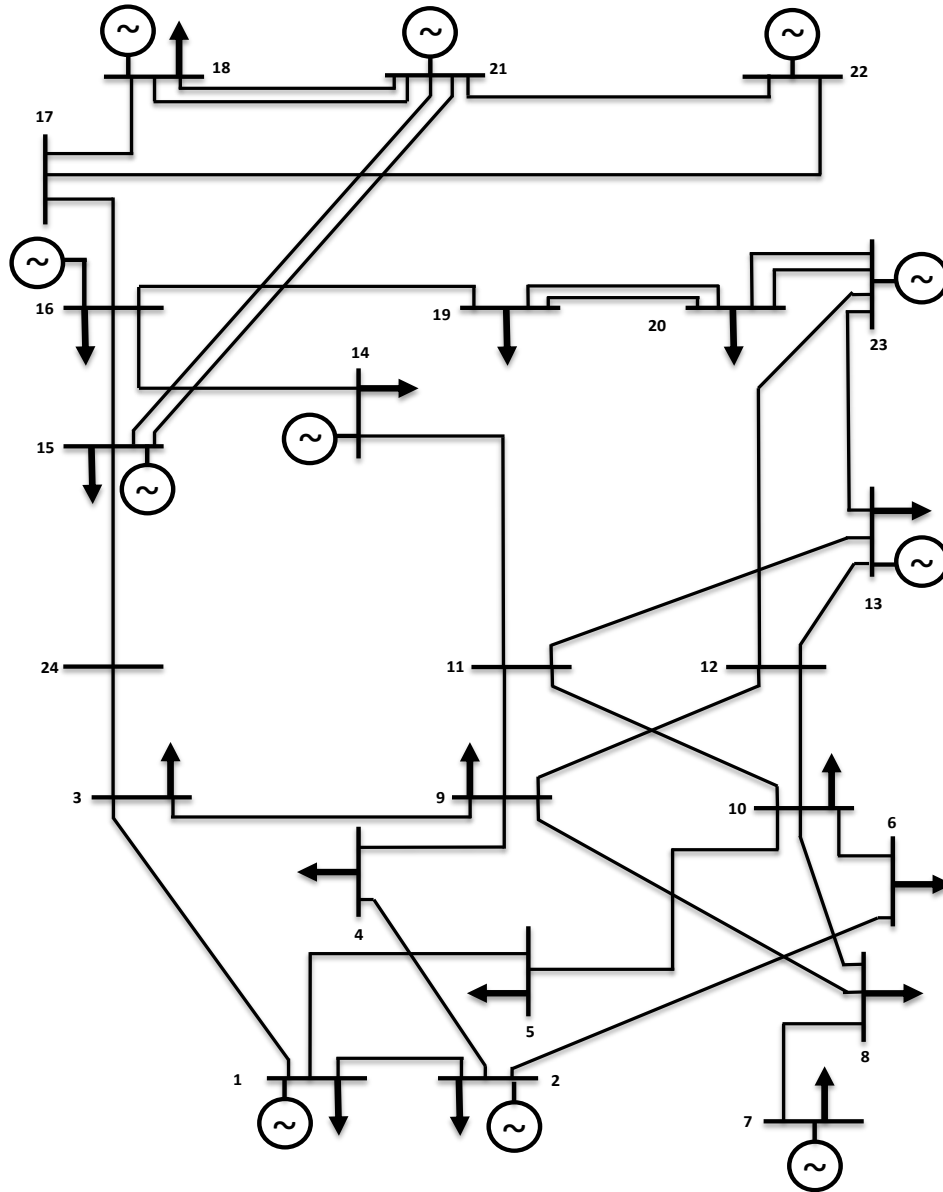


**Figure 1.10:** IEEE 24 bus test system

The prices of the three fuel types together with the system demand are four changing parameters in the OPF problem. Therefore, multi-linear interpolation on a 4-dimensional lattice is employed to estimate the hourly operation cost of the system. To compute the

**Table 1.7:** Data associated to the parallel elements for 24 bus system

Line (from-to)	X (p.u)	Capacity (MW)	IC (M\$)	Line (from-to)	X (p.u)	Capacity (MW)	IC (M\$)
1-2	0.0139	175	1.575	9-12	0.0839	400	3
1-3	0.2112	175	2.8875	10-11	0.0839	400	3
1-5	0.0845	175	1.155	10-12	0.0839	400	3
2-4	0.1267	175	1.7325	11-13	0.0476	500	1.98
2-6	0.192	175	2.8875	11-14	0.0418	500	1.74
3-9	0.119	175	1.6275	12-13	0.0476	500	1.98
3-24	0.0839	400	3	12-23	0.0966	500	4.02
4-9	0.1037	175	1.4175	13-23	0.0865	500	3.6
5-10	0.0883	175	1.2075	14-16	0.0389	500	1.62
6-10	0.0605	175	8.4	15-16	0.0173	500	0.72
7-8	0.0614	175	8.4	15-21	0.049	500	0.72
8-9	0.1651	175	2.2575	15-21	0.049	500	4.08
8-10	0.1651	175	2.2575	15-24	0.0519	500	2.16
9-11	0.0839	400	3	16-17	0.0259	500	2.28
16-19	0.0231	500	0.96	17-18	0.0144	500	0.6
17-22	0.1053	500	0.438				

**Table 1.8:** Annual average fuel price

Fuel type	<i>Year</i> <sub>1</sub>	<i>Year</i> <sub>2</sub>	<i>Year</i> <sub>3</sub>	<i>Year</i> <sub>4</sub>	<i>Year</i> <sub>5</sub>	<i>Year</i> <sub>6</sub>	<i>Year</i> <sub>7</sub>	<i>Year</i> <sub>8</sub>	<i>Year</i> <sub>9</sub>	<i>Year</i> <sub>10</sub>
Oil(\$/barrel)	22.97	26.39	30.31	34.82	40.00	45.95	52.78	60.63	69.64	80.00
Natural gas(\$/Mcf)	6.89	7.91	9.09	10.47	12	13.78	15.83	18.18	20.89	24
Coal(\$/ton)	43.00	47.00	51.00	52.00	54.00	56.00	58.00	62.00	66.00	69.00

**Table 1.9:** The peak demand data for each year of the 10-year horizon period

<i>Year</i> #	Bus #																
	1	2	3	4	5	6	7	8	9	10	13	14	15	16	18	19	20
1	116.33	104.49	193.9	140.52	76.48	146.5	140.15	184.19	188.5	210.04	285.41	282.9	341.43	324.82	358.66	303.86	167.21
2	125.63	112.83	209.39	86.08	82.58	158.19	149.71	198.9	203.56	226.81	308.26	306.32	368.72	305.8	387.36	381.69	209.35
3	135.68	121.85	226.15	212.6	89.19	170.87	170.67	214.84	219.87	244.99	332.93	327.21	398.23	380.87	418.38	413.81	192.71
4	146.55	131.6	244.23	231.84	96.34	184.53	183.7	232	237.44	264.59	359.55	356.77	430.08	337.45	451.8	442.16	243.45
5	158.26	142.15	263.79	204.76	104.05	199.3	186.05	250.6	256.42	285.75	388.35	385.26	464.55	447.35	488	456.31	263.49
6	170.92	153.5	284.89	221.28	112.36	215.25	215.02	270.63	276.96	308.62	419.41	404.9	501.71	444.9	527.01	517.45	283.21
7	184.6	165.8	307.64	235.37	121.36	232.46	218.32	292.24	299.08	333.29	452.92	409.22	541.72	505.39	569.13	542.47	262.86
8	199.36	179.05	332.26	280.1	131.03	250.98	230.72	315.63	323.05	359.88	489.15	387.93	585.15	557.78	614.72	600.61	324.21
9	215.31	193.38	358.86	306.71	141.54	271.13	249.2	340.88	348.89	388.76	528.33	527.53	631.89	625.15	663.81	617.06	326.76
10	225.3	203.34	368.85	209.23	151.52	281.1	259.19	350.88	358.89	398.76	538.33	418	642	579.76	673.9	668.75	370.57

estimation error for a random sample of 1000 points from each data range, we computed the operation cost by the multivariate interpolation and the OPF problem for the chosen points. The estimation error (MAE) for the described sample, considering 5 breakpoints, is 0.04%.

### 1.5.5 Comparing the results of the proposed and traditional methods

We ran the BPSO algorithm for 100 iterations. In either method, after 82 iterations, no considerable change in the objective function value was observed. To determine the number of breakpoints for the multivariate interpolation, we set the maximum allowed computational time of the algorithm to one week. As it takes 0.15 seconds on average to solve the OPF problem for the IEEE 24-bus test system, the number of breakpoints using (36) was computed to be 5. The algorithm's run time for the proposed method was 6 days and 13 hours and for the traditional method was 4 hours and 16 minutes on a 3 GHz Core 2 Duo processor. The number of particles was assumed to be 30. The number and the location of the newly added circuits are different in the obtained plans by the proposed and traditional methods. In the final plan obtained by the proposed and traditional methods, seven and eight new circuits, respectively, are added to the transmission network. The newly added circuits to the 24-bus system based on both methods have been shown in Table 1.10. To compare the total cost of the two methods, we computed the hourly operation cost by solving the OPF problem at each hour for both plans. Table 1.11 summarizes the present worth of the annual operation and investment costs for the final plans. The total cost of the multivariate interpolation is \$4.42M less than the traditional plan.

### 1.5.6 Expansion planning for real-world power systems

The proposed method has the potential for use in real-world transmission expansion problems since the computational effort depends mostly on the number of OPF problems that need to be solved. The number of OPF problems can be selected by trading off the number of breakpoints and the accuracy of the total operational cost. When the number of breakpoints is decreased, the computational time will consequently decrease and the TEP problem could be solved for a real-world problem in a reasonable time. To further reduce the computational time, we can decrease the maximum allowed number of circuits at each line and use more powerful processors or parallel processing. For the real-world problems, when

**Table 1.10:** Added lines to the 24 bus network based on the proposed and traditional methods

Method	Line (from-to)	Year <sub>1</sub>	Year <sub>2</sub>	Year <sub>3</sub>	Year <sub>4</sub>	Year <sub>5</sub>	Year <sub>6</sub>	Year <sub>7</sub>	Year <sub>8</sub>	Year <sub>9</sub>	Year <sub>10</sub>	Total
Multivariate Interpolation	11-14	1										1
	15-16		1									1
	16-17			1								1
	17-22		1	1								2
	14-16	1			1							2
OPF Problem	11-14	1										1
	15-16				1							1
	15-21					1						1
	16-17		1									1
	14-16	1				1						2
	17-22					1		1				2

**Table 1.11:** The annual operation and investment costs for IEEE 24 bus system

Method	Demand	Fuel price	Cost type	Year <sub>1</sub>	Year <sub>2</sub>	Year <sub>3</sub>	Year <sub>4</sub>	Year <sub>5</sub>	Year <sub>6</sub>	Year <sub>7</sub>	Year <sub>8</sub>	Year <sub>9</sub>	Year <sub>10</sub>	Total
Multivariate Interpolation	Hourly	Daily price	Operation cost (\$100 M)	3.5635	3.6167	3.6357	3.8001	3.9250	4.0502	4.1641	4.2614	4.3871	4.1221	39.5259
			Investment cost	0.0162	0.0158	0.0036	0.0087	0.0266	0	0	0	0	0	0
		Total	3.5797	3.6325	3.6393	3.8088	3.9516	4.0502	4.1641	4.2614	4.3871	4.1221	39.5979	
OPF problem	Peak	Annual price	Operation cost (\$100 M)	3.5655	3.6167	3.6554	3.7996	3.9437	4.0494	4.1641	4.2614	4.3879	4.1240	39.5678
			Investment cost	0.0162	0.0158	0.0188	0	0	0.0127	0.0406	0.0224	0.0335	0	0
		Total	3.5817	3.6325	3.6743	3.7996	3.9437	4.0622	4.1682	4.2637	4.3913	4.1240	39.6411	

the likelihood of having a line between two buses is too low, we can disregard that candidate line. The reduction in the number of candidate lines will reduce the BPSO algorithm's run time.

## 1.6 Conclusion

In this research, we introduced a new method to solve the multiyear security constrained TEP problem. In contrast to traditional methods in which the operation cost is typically computed for the peak demand, we compute it for the hourly demand over the planning horizon. In addition, we used daily fuel prices. We proposed a multilinear interpolation method to compute the hourly operation cost. The main advantage of using the multivariate interpolation is reduction on the computational time. The computational time showed a reduction factor of 70 for the Garver's 6-bus system with three changing parameters and a reduction factor of 15 for the IEEE 24-bus system with four changing parameters. In order to validate the interpolation method, we compared its results to those of the OPF problem. The error of the interpolated values was less than 0.02%. The BPSO algorithm was employed to solve the TEP problem. We applied our method to the Garver's 6-bus and the IEEE 24-bus test systems for a planning horizon of ten years. For real-world power systems, we made a few suggestions on how to reduce the computational time of the proposed method. The proposed method was compared with a traditional method based on the total cost of the final expansion plan. In the traditional method, the peak demand instead of hourly demand and annual average instead of daily fuel price were considered. The comparison results revealed that the expansion plan obtained by the proposed method is more economical than traditional methods in terms of investment and operation costs.

## References

- [1] A.S.D. Braga and J.T. Saraiva, “A Multiyear Dynamic Approach for Transmission Expansion Planning and Long-Term Marginal Costs Computation”, *IEEE Transactions on Power Systems*, vol. 20, no. 3, pp. 1631-1639, 2005.
- [2] H. Zhang, V. Vittal, G.H. Thomas and J. Quintero, “A Mixed-Integer Linear Programming Approach for Multi-Stage Security-Constrained Transmission Expansion Planning”, *IEEE Transactions on Power Systems*, vol. 27, no. 2, pp. 1125-1133 , 2012.
- [3] Y. Jin, H. Cheng, J. Yan and L. Zhang, “New discrete method for particle swarm optimization and its application in transmission network expansion planning”, *Electric Power Systems Research*, vol. 77, no. 3, pp. 227-233, 2007.
- [4] H.A. Gil and E.L. da Silva, “A reliable approach for solving the transmission network expansion planning problem using genetic algorithms”, *Electric Power Systems Research* , vol. 58, no. 1, pp. 45-51, 2001.
- [5] V.H. Hinojosa, N. Galleguillos and B. Nuques, “A simulated rebounding algorithm applied to the multi-stage security-constrained transmission expansion planning in power systems”, *International Journal of Electrical Power and Energy Systems*, vol. 47, pp. 168-180, 2013.
- [6] J.A. Aguado, S. dela Torre, J. Contreras, A.J. Conejo and A. Martinez, “Market-driven dynamic transmission expansion planning”, *Electric Power Systems Research*, vol. 82, pp. 88-94, 2012.

- [7] G. A. Orfanos, P. Georgilakis and N. D. Hatziargyriou, "Transmission expansion planning of systems with increasing wind power integration", *IEEE Transactions on Power Systems*, vol. 28, no. 2, pp. 1355-1362, 2013.
- [8] R. Hemmati, R. Hooshmand and A. Khodabakhshian , "State-of-the-art of transmission expansion planning: Comprehensive review", *Renewable and Sustainable Energy Reviews*, vol. 23, pp. 312-319, 2013.
- [9] M. S. Sepasian, H. Seifi, A. Akbari Foroud and A. R. Hatami, "A multiyear security constrained hybrid generation-transmission expansion planning algorithm including fuel supply costs", *IEEE Transactions on Power Systems*, vol. 24, no. 3, pp. 1609-1618, 2009.
- [10] I. Sharan and R. Balasubramanian, "Integrated generation and transmission expansion planning including power and fuel transportation constraints", *Energy Policy*, vol. 43, pp. 275-284, 2012.
- [11] H. Arsham and M. Oblak, "Perturbation analysis of general LP models: A unified approach to sensitivity, parametric, tolerance, and more-for-less analysis", *Mathematical and Computer Modeling*, vol. 13, no. 8, pp. 79-102, 1990.
- [12] R.E. Wendell, "The tolerance approach to sensitivity analysis in linear programming", *Management Science*, vol. 31, no. 5, pp. 564-578, 1985.
- [13] H. Greenberg, "Simultaneous primal-dual right-hand-side sensitivity analysis from a strictly complementary solution of a linear program", *SIAM Journal on Optimization*, vol. 10, no. 2, pp. 427-442, 2000.
- [14] R. S. Chanda and P. K. Bhattacharjee, "Application of computer soft-ware in transmission expansion planning using variable load structure", *Electric Power Systems Research*, vol. 31, pp. 13-20, 1994.

- [15] K. J. Kim, Y. M. Park and K. Y. Lee, "Optimal long term transmission expansion planning based on maximum principle", *IEEE Transactions on Power Systems*, vol. 3, pp. 1494-1501, 1988.
- [16] L. L. Garver, "Transmission network estimation using linear programming", *IEEE Transactions on Power Apparatus and Systems*, vol. 7, pp. 1688-1697, 1970.
- [17] Y. P. Dusonchet and A. H. El-Abiad, "Transmission planning using discrete dynamic optimization", *IEEE Transactions on Power Apparatus and Systems*, vol. 4, pp. 1358-1371, 1973.
- [18] H. K. Youssef and R. Hackam, "New transmission planning model", *IEEE Transactions on Power Systems*, vol. 4, pp. 9-18, 1989.
- [19] L. Bahiense, G. C. Oliveira, M. Pereira and S. Granville, "A mixed integer disjunctive model for transmission network expansion", *IEEE Transactions on Power Systems*, vol. 16, pp. 560-565, 2001.
- [20] S. Binato, M. V. F. Pereira and S. Granville, "A new Benders decomposition approach to solve power transmission network design problems ", *IEEE Transactions on Power Systems*, vol. 16 , pp. 235-240, 2001.
- [21] P. Tsamasphyru, A. Renaud and P. Carpentier, "Transmission network planning: An efficient Benders decomposition scheme", *Proceedings of the 13th PSCC*, pp. 487-494, 1999.
- [22] R. Romero and A. Monticelli, "A hierarchical decomposition approach for transmission network expansion planning", *IEEE Transactions on Power Systems*, vol 9, pp. 373-380, 1994.
- [23] H. Rudnick, R. Palma, E . Cura and C. Silva , " Economically adapted transmission systems in open access schemes-application of genetic algorithms", *IEEE Transactions on Power Systems*, vol. 11, no. 3, pp. 1427-1440, 1996.

- [24] E. Sauma and S. Oren, "Economic criteria for planning transmission investment in restructured electricity markets", *IEEE Transactions on Power Systems*, vol. 22, no. 4, pp. 1394-1405, 2007.
- [25] A.L. da Silva, L. Rezende, L. H. andrio and L. Manso, "Performance comparison of metaheuristics to solve the multi-stage transmission expansion planning problem", *IET generation transmission and distribution*, vol. 5, no. 3, pp.360-367, 2011.
- [26] R.S. Chanda and P.K. Bhattacharjee, "A reliability approach to transmission expansion planning using fuzzy fault-tree model", *Electric Power Systems Research*, vol. 45, no. 2, pp. 101-108, 1998.
- [27] M.C. da Rocha and J. Saraiva, "A multiyear dynamic transmission expansion planning model using a discrete based on EPSO approach", *Electric Power Systems Research*, vol. 93, pp. 83-92, 2012.
- [28] M. C. da Rocha and J. T. Saraiva, "A discrete evolutionary PSO based approach to the multiyear transmission expansion planning problem considering demand uncertainties", *International Journal of Electrical Power and Energy Systems*, vol. 45, no. 1, pp. 427-442, 2013.
- [29] H. Shayeghi, M. Mahdavi and A. Bagheri, "Discrete PSO algorithm based optimization of transmission lines loading in TNEP problem", *Energy Conversion and Management*, vol. 51, no. 1, pp. 112-121, 2010.
- [30] L. F. Fuerte-Ledezma, G. Gutierrez-Alcaraz and M. S. Javadi, "Static transmission expansion planning considering uncertainty in demand using BPSO", *North American Power Symposium (NAPS)*, IEEE, pp. 1-6, 2013.
- [31] A. Kimiyaghalam, M. Mahdavi, S. Jalilzadeh and A. Ashouri, "Improved Binary Particle Swarm Optimization Based TNEP Considering Network Losses, Voltage Level, and Uncertainty in Demand", *Journal of Artificial Intelligence in Electrical Engineering*, vol. 1, no. 2, pp. 29-42, 2012.

- [32] N. Alguacil, A.L. Motto and A. Conejo, "Transmission Expansion Planning: A Mixed-Integer (LP) Approach ", *IEEE Transactions on Power Systems*, vol. 18, no. 3, pp. 1070-1077, 2003.
- [33] T. Akbari and M.Tavakoli Bina, "A linearized formulation of AC multi-year transmission expansion planning: A mixed-integer linear programming approach", *Electric Power Systems Research*, vol. 114, pp. 93-100, 2014.
- [34] A. J. Wood and B. F. Wollenberg " Power generation, operation, and control ", *John Wiley and Sons*, 2012.
- [35] F. Alvarado and S. Oren, " Transmission system operation and interconnection ", *National transmission grid study-Issue papers*, pp. A1-A35, 2002.
- [36] G. Kamyab, M. Fotuhi-Firuzabad, M. Rashidinejad, "A PSO based approach for multi-stage transmission expansion planning in electricity markets ", *International Journal of Electrical Power and Energy Systems*, vol. 54, pp. 91-100, 2014.
- [37] J. Kennedy and R.C. Eberhart, "A discrete binary version of the particle swarm algorithm", *Systems, Man, and Cybernetics, Computational Cybernetics and Simulation*, vol. 5, pp. 4104-4108, 1997.
- [38] M. A. Khanesar, H. Tavakoli and M.Teshnehlab and M.A. Shoorehdeli, "A discrete binary version of the particle swarm algorithm", *IEEE Mediterranean Conference in Control and Automation*,, pp. 1-6, 2007.
- [39] Y. Shi and R. Eberhart, "A modified particle swarm optimizer", *IEEE World Congress on Computational Intelligence on Evolutionary Computation Proceedings*, pp. 69-73, 1998.
- [40] R. Wagner, "Multi-Linear Interpolation", *Beach Cities Robotics*, 2008.
- [41] M.D. Gay, "IBM ILOG CPLEX Optimization Studio CPLEX Use's Manual", *International Business Machines Corporation*, ed. 12.4, 2012.

- [42] Subcommittee, “IEEE reliability Test system”, *IEEE Transactions on Power Apparatus and Systems*, pp. 2047-2054, 1979.
- [43] “ U.S. Energy Information Administration (EIA) ”, <http://www.eia.gov>, 2013.

## Chapter 2

### Microgrid Energy Scheduling Using Storage from Electric Vehicles

#### 2.1 Abstract

Integrating electric vehicles (EVs) into a microgrid can provide additional energy and storage to the microgrid. The benefits depend on factors such as market prices, EVs' state of charge, and their arrival/departure times. In this chapter, it is assumed that the microgrid operates in a grid-connected mode and consists of thermal units, renewable energy resources and a parking facility. An optimization model for the energy scheduling that considers the energy and storage provided by the EVs is proposed. The objective function of the model is to minimize the expected total operation costs including generation, day-ahead market, battery wear, and real-time balancing costs for the next 24hrs. The uncertainty of the demand and the available EVs in addition to the intermittency of the renewable energy resources are taken into account. The model is solved using the Benders' decomposition algorithm and results are obtained using a 14-bus distribution test system. The results show that using the storage and energy of the EVs reduces the total operation cost of the microgrid.

**Keywords:** Microgrid, Electric vehicles, Energy storage, Uncertainty, Benders' decomposition, Day-ahead energy market

#### 2.2 Introduction

The development of microgrids has sparked significant interest in recent years because of the potential to improve the reliability of the electric power system [1]. When the power

grid fails to deliver electricity, microgrids can operate independently and fulfill the demand within their boundaries. In addition to improving reliability, a microgrid can reduce the cost of energy by increasing local load control, integrating different sources of renewable energy and trading energy in the electricity market. In [2], several market-based pricing models were studied to minimize the cost of electricity in microgrids. The experimental results showed that by using a sustainable microgrid, the energy cost of residential consumers can be reduced by 20%.

The electric vehicle (EV) is another entity that can exchange energy in the electricity market and contribute to the economic aspects of power systems. To allow EVs to exchange energy with electricity markets, aggregators and microgrids can serve as an interface [2]. Several studies have analyzed the interaction between aggregators and EVs. In [10], an aggregator collected the demand of EV fleets and purchased electricity from the energy market on their behalf. The study compared the impact of centralized and decentralized charging schemes on the system-wide generation cost. In another article [11], the authors developed an optimal bidding strategy for the EV aggregator in the day-ahead energy market. The goal was to minimize charging cost while meeting the uncertain demand of the EVs in real time. In [6], a similar framework was proposed for an EV aggregator to purchase energy for the EV owners based on the forecasted power price and the EVs' demand. In [7], the EV aggregator used energy storage devices to mitigate the impact of uncertainty and inaccurate prediction in real time. In these studies, the primary objective of the aggregator was charging the EVs at a minimum cost. The EV batteries were not exploited as a storage resource for improving the economics of the charging system.

A microgrid can also act as an EV aggregator and integrate the EVs into the system. In [8], the authors developed an electricity and heat generation schedule that was coordinated with the EVs' charging schedule in a microgrid. In [9], the plug-in hybrid electric vehicles (PHEV) were integrated into an office building microgrid and the effect of different charging ratings was studied. In [10] a model was proposed to simulate a solar parking lot for EVs.

The authors used queuing theory to model the vehicles' arrivals and departures. The excess energy was exported to the grid and the excess EV demand was imported from the grid. In all of these studies, the microgrid integrated the EVs but did not use the storage capacity of the EVs.

Using storage capacity of the EVs in microgrids has also been considered. In [11], the coordination of the PEV charging/discharging schedule with volatile wind power to optimize the energy dispatching in a microgrid was studied. The coordination goal was balancing the power generation and demand in real time. In [8], a new method for optimal integration of PHEVs in microgrids was introduced. The proposed method determined the optimal parking capacity for the EVs in the microgrid. The authors used the EVs' batteries to store energy. However, they never considered the EV owners' benefits, the stochastic aspect of the storage capacity provided by the EVs and the power flow constraints.

The energy management problem for a microgrid has also been studied. A stochastic energy management model for microgrids in which the storage devices and the EV demand are integrated to the system has been proposed in [13]. The EVs were considered as a local load and the real-time energy imbalances were not considered. In [14] the authors solved a similar model including the real-time imbalances without considering economic dispatch. In all of the microgrid studies, the variability and uncertainty aspects of the storage capacity provided by the EVs have been neglected. Also, the integration benefits and the cost of power imbalances in real time have not been considered.

In this chapter, we propose a mathematical model for managing the energy in a grid-connected microgrid that includes different sources of energy and a parking facility for EVs. The parking facility, due to its ability to accommodate a significant number of EVs, can supply a substantial amount of energy and battery capacity to the microgrid. By using the EVs' storage capacity, the microgrid can import energy to be consumed or stored in the EVs' batteries during hours of low electricity prices; thereby reducing the need to purchase power at high-price hours. The energy stored in the EVs can be discharged using a vehicle to grid

(V2G) program at hours of high prices. We also assume that the microgrid does not operate as a commercial charging station. That is, the energy level of an EV at departure would be equal to its energy level upon arrival. The EV owners are compensated by obtaining access to free parking and cash for battery wear. Since there is no contractual obligation, EV owners can choose to participate in other markets or demand response programs that may provide higher benefits. Exploiting the energy and storage capacity can be complicated. For instance, if the battery of an arriving EV is full and the owner decides to depart shortly at a high price hour, discharging that EV's battery might not be economically justified. We propose an optimization model that enables the microgrid to manage the battery capacity and energy content of the parked EVs. The energy management decisions are made based upon a two-stage stochastic optimization model. The model makes first stage decisions a day ahead according to the available data and determines the behavior of the microgrid in the operation day after the uncertain data are revealed. We assume that the microgrid operator makes an arrangement with a local power distributor to export and import excess supply or demand in real time at fixed prices. The contributions of this chapter are:

1. A mathematical model to manage the energy within a grid-connected microgrid.
2. A model that considers the variable and uncertain storage capacity of the EVs' parking facility.
3. An extensive analysis to assess the economic effects of integrating the parking facility into the microgrid.
4. A cost saving mechanism to improve the economic benefits of the integration

The remainder of this chapter is organized as follows: Section 2.3 presents the problem description. Section 2.4 proposes the mathematical formulation of the problem. Section 2.5 details the solving algorithm and Section 2.6 explains the stochastic modeling of the energy storage. Section 2.7 discusses a microgrid case study. Section 2.8 shows the simulation results and Section 2.9 draws the conclusions.

## 2.3 Problem Description

Microgrids are usually composed of distributed generation units, local loads and a central control unit that operates in accordance with the power grid. Smart Microgrids are able to efficiently and economically satisfy the consumers' demands within their boundaries. In addition, they can provide several opportunities for the consumers to participate in microgrids' energy scheduling, deliver demand response services for the grid and trade energy in the energy market to improve the environmental and economic benefits. In this chapter, we assume a microgrid consisting of conventional thermal units, small scale wind turbines, solar panels and an EV parking facility. The microgrid is connected to the power grid and can exchange energy in the electricity market. The microgrid operator determines the commitment status of the thermal units and the amount of energy to be purchased or sold in the day-ahead market. Due to the stochastic nature of the loads, the storage capacity and the output of the renewable resources, there will be some discrepancies between the forecasted demand and supply and their actual quantities. To resolve the imbalance between demand and supply, we assume that the microgrid operator agrees with a power distributor to exchange excess supply or demand for fixed predefined prices. A contract with a power distributor at a fixed price hedges against the highly volatile prices of the real-time market.

### 2.3.1 Modeling Uncertainty

The energy management problem is formulated as a two stage stochastic optimization model. In the first stage, the price of energy in the day-ahead market is forecasted and the contracted prices with the power distributor are assumed to be known. In this stage, the optimal commitment schedule of the thermal units and the energy purchases or sales in the day-ahead market are determined. In the second stage, the net demand and the battery of the parking facility are modeled as stochastic parameters. To represent these, we generate scenarios for each parameter. In this stage, charging/discharging schedule of EVs, balancing activities and generation dispatch are determined for each scenario.

### 2.3.2 Parking Facility

In addition to power resources, the microgrid uses an EV parking facility equipped with a bidirectional flow capability to perform a V2G program. The parking facility is assumed to be a virtual battery whose capacity depends on the batteries of the available EVs in the parking. This capacity is variable as the available number of EVs in the parking facility changes over time, and it is stochastic as the arrivals and departures of the EVs to/from the parking facility are not known with certainty.

## 2.4 Problem Formulation

The formulation of the energy management problem includes the objective function and all of the system constraints.

### 2.4.1 Objective Function

The objective function is given in (2.1) and minimizes the expected total operation cost of the microgrid. The total cost includes the costs of first stage decisions and the expected cost of the second stage decisions over all scenarios. The first stage costs are the cost of energy purchases and sales in the day-ahead market and startup and shutdown costs of the thermal units. The second stage costs are the generation cost of the thermal units, cost of battery wear and the cost of power exchanges (balancing) with the local power distributor at each scenario  $s$ .

$$\text{Min } z = \sum_t (P_t^{da} x_t) + \sum_t \sum_j (s_{jt}^{up} + s_{jt}^{sd}) + \sum_t \sum_s \pi_s \sum_j (c_j^f f_{jt,s} + \gamma(y_{t,s}^+ + y_{t,s}^-) + \varphi z_{t,s}) \quad (2.1)$$

### 2.4.2 Constraints

Constraints in (2.2) ensure that the power supply and demand at each hour for each scenario are balanced. As the wind and solar energy resources are assumed to be non-dispatchable, they are shown as negative loads [15].

$$\sum_j a_{jt,s} + x_t + z_{t,s} - y_{t,s}^+ + y_{t,s}^- = P_{t,s}^{loss} + D_{t,s} - W_{t,s} - S_{t,s} \quad \forall t, \forall s \quad (2.2)$$

As noted, we model the parking facility as a single battery with a capacity equal to the sum of the capacity of all batteries in the parking facility. The total capacity will change over time because of the variable number of available EVs in the parking. Equations (2.3) and (2.4) represent the maximum and minimum capacity of the parking facility at hour  $t$ .

$$E_{t,s}^{min} = E_{t-1,s}^{min} + E^{min}(\beta(N_{t,s}^{arr} - N_{t,s}^{dep})) \quad \forall t, \forall s \quad (2.3)$$

$$E_{t,s}^{max} = E_{t-1,s}^{max} + E^{max}(\beta(N_{t,s}^{arr} - N_{t,s}^{dep})) \quad \forall t, \forall s \quad (2.4)$$

The added and deducted energy to/from the parking battery at time  $t$  is presented in (2.5) and (2.6). It is assumed that the microgrid returns the borrowed energy from the EVs at departure. Therefore, the energy content of the departing EVs will be equal to their energy content at arrival.

$$E_{t,s}^{arr} = SOC[(\beta N_t^{arr})] \quad \forall t, \forall s \quad (2.5)$$

$$E_{t,s}^{dep} = SOC[(\beta N_t^{dep})] \quad \forall t, \forall s \quad (2.6)$$

The total energy content of the parking battery at time  $t$  is given by (2.7) and it is constrained in (2.8) to the minimum and maximum capacity of the parking battery at that

time.

$$e_{t,s} = e_{t-1,s} + (1/\eta_d)E_{t,s}^{arr} - (\eta_c)E_{t,s}^{dep} + \eta_c y_{t,s}^+ - (1/\eta_d)y_{t,s}^+ \quad \forall t, \forall s \quad (2.7)$$

$$E_{t,s}^{min} \leq e_{t,s} \leq E_{t,s}^{max} \quad \forall t, \forall s \quad (2.8)$$

The maximum energy that can be stored or withdrawn from the battery at each hour is also constrained by the rated capacity of the charger and given by (2.9) to (2.11).

$$h_{t,s}^+ + h_{t,s}^- \leq 1 \quad \forall t, \forall s \quad h_{t,s}^+ \& h_{t,s}^- \in \{0, 1\} \quad (2.9)$$

$$0 \leq y_{t,s}^+ \leq h_{t,s}^+ \cdot CH^{max} \sum_{k=1}^t (N_{k,s}^{arr} - N_{k,s}^{dep}) \quad \forall t, \forall s \quad (2.10)$$

$$0 \leq y_{t,s}^- \leq h_{t,s}^- \cdot CH^{max} \sum_{k=1}^t (N_{k,s}^{arr} - N_{k,s}^{dep}) \quad \forall t, \forall s \quad (2.11)$$

The thermal unit commitment constraints are given by (2.12) to (2.21):

$$s_{jt}^u \geq S_j^{up}(u_{jt} - u_{jt-1}); s_{jt}^u \geq 0 \quad \forall t, \forall j \quad (2.12)$$

$$s_{jt}^d \geq S_j^{dn}(u_{jt-1} - u_{jt}); s_{jt}^d \geq 0 \quad \forall t, \forall j \quad (2.13)$$

$$\sum_{t=k}^{k+UT_j-1} u_{jt} \geq UT_j(u_{jk} - u_{jk-1}) : \quad \forall j, k = 2, \dots, T - UT_j + 1 \quad (2.14)$$

$$\sum_{t=k}^T (u_{jt} - (u_{jk} - u_{jk-1})) \geq 0 \quad \forall j, k = T - UT_j + 2, \dots, T \quad (2.15)$$

$$\sum_{t=k}^{k+DT_j-1} (1 - u_{jt}) \geq DT_j(u_{jk-1} - u_{jk}) \quad \forall j, k = 2, \dots, T - DT_j + 1 \quad (2.16)$$

$$\sum_{t=k}^T (1 - u_{jt} - (u_{jk} - u_{jk-1})) \geq 0 \quad \forall j, k = T - DT_j + 2, \dots, T \quad (2.17)$$

$$a_{jt,s} - a_{jt-1,s} \leq R_j^u(u_{jt} - 1) \quad \forall t, \forall j, \forall s \quad (2.18)$$

$$a_{jt-1,s} - a_{jt,s} \leq R_j^d(u_{jt}) \quad \forall t, \forall j, \forall s \quad (2.19)$$

$$f_{jt,s}(HV_j) = a_{jt,s}(HR_j) \quad \forall t, \forall j, \forall s \quad (2.20)$$

$$u_{jt} \cdot A_j^{min} \leq a_{jt,s} \leq u_{jt} \cdot A_j^{max} \quad \forall t, \forall j, \forall s \quad (2.21)$$

And the power flow constraints are given by (2.22) to (2.27):

$$\sum_n (V_{it,s} \cdot V_{nt,s} \cdot (G_{in} \cdot \cos(\delta_{it,s} - \delta_{nt,s}) + B_{in} \cdot \cos(\delta_{it,s} - \delta_{nt,s}))) = P_{it,s}^{net} + P_{i,s}^{slack} \quad \forall i, \forall t, \forall s \quad (2.22)$$

$$\sum_n (V_{it,s} \cdot V_{nt,s} \cdot (G_{in} \cdot \sin(\delta_{it,s} - \delta_{nt,s}) + B_{in} \cdot \cos(\delta_{it,s} - \delta_{nt,s}))) = Q_{it,s}^{net} + Q_{i,s}^{slack} \quad \forall i, \forall t, \forall s \quad (2.23)$$

$$|S_{int,s}| \leq S_{in}^{max} \quad \forall n, i = 1, \dots, N, \forall t, \forall s \quad (2.24)$$

$$V_n^{min} \leq V_{nt,s} \leq V_n^{max} \quad \forall n, \forall t, \forall s \quad (2.25)$$

$$\delta^{min} \leq \delta_{nt,s} \leq \delta^{max} \quad \forall n, \forall t, \forall s \quad (2.26)$$

$$x_t, z_{t,s} \in \{-\infty, +\infty\}, \quad u_{j,t} \in \{0, 1\} \quad (2.27)$$

## 2.5 Solving Algorithm

The proposed energy management model (2.1) to (2.27) is a MINLP problem which is complicated to solve. There are multiple methods to solve this type of problem. We have chosen the Benders' decomposition approach (BDA) because of the successful application of BDA in [19] and the block angular structure the constraint matrix which makes it a good candidate for the BDA. In applying the BDA, the original problem is decomposed into a master problem and a sub-problem. After the master problem is solved, its solution is examined in the sub-problem. If the sub-problem is infeasible, a Bender's cut is added to the master problem. This process will iterate until the solution converges [17]. To solve the

proposed model with BDA based on [19], we partition the problem into two problems: a master problem and a sub-problem. The master problem includes the entire model without the AC-OPF constraints (2.22) to (2.27). The sub-problem includes the AC-OPF constraints. To solve the master problem, we use the IBM ILOG CPLEX interactive optimizer with Concert technology in C++ [19]. We use Matpower 5.1 [21] to solve the sub-problem. Figure 2.1 illustrates the software interaction to solve the proposed Benders' decomposition.

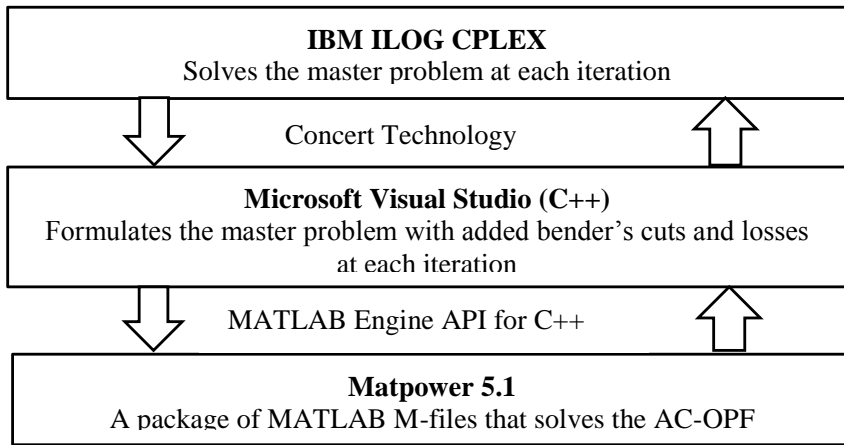


**Figure 2.1:** Software interaction to solve the Benders' decomposition

As in [19], we add slack active and reactive power variables (virtual generation  $P_{i,s}^{slack}, Q_{i,s}^{slack}$ ) to the active and reactive power flow constraints to make the power flow equations always feasible. We then set a positive cost ( $M$ ) for the output of the virtual generators to penalize the objective function of the AC-OPF problem. The objective function of the AC-OPF is presented in (2.28). Note that we have penalized the active power variables in the objective function.

$$\min w_{t,s} = \sum_i = M(P_{i,s}^{slack}) \quad \forall t, \forall s \quad (2.28)$$

At each iteration of the BDA, the AC-OPF is solved for each scenario and the shadow prices associated with the injected active power from each thermal unit ( $\lambda_{jt,s}$ ), the parking battery ( $\psi_{t,s}$ ), and the power distributor ( $\zeta_{t,s}$ ) are determined. We also obtain the power losses at every dispatch. The Benders' cuts (2.29) are added to the master problem at iteration  $k$ . In (2.28),  $w_{t,s}$  is the objective function of the AC-OPF problem,  $A_{jt,s}^k, Y_{t,s}^k, Z_{t,s}^k$  are the output of the master problem for the thermal units' generated energy, the energy withdrawn from the parking battery and the purchased energy from the power distributor, respectively. The  $w^*$  is added to the objective function of the master problem at iteration  $k$ . We also add the power losses to (2.2). Without adding the losses, the power losses would be compensated using the virtual generators and the algorithm will never converge.

$$w^* \geq w(A_{jt,s}^k, Y_{t,s}^k, Z_{t,s}^k) + \sum_j \lambda_{jt,s} (a_{jt,s}^k - A_{jt,s}^k) + \psi_{t,s} (y_{t,s}^k - Y_{t,s}^k) + \zeta_{t,s} (z_{t,s}^k - Z_{t,s}^k) \quad \forall j, \forall t, \forall s \quad (2.29)$$

The AC-OPF is solved at each hour for each scenario. If the output of the virtual generators is greater than zero, a Benders' cut is added to the master problem. The solving algorithm is presented in Figure 2.2. The algorithm will iterate until the solution of the sub-problem does not change.

## 2.6 Stochastic Modeling of the Energy Storage

Due to the variability and uncertainty of the arrivals and departures over time, the storage capacity provided by the EVs in the parking facility is variable and uncertain. To model the arrivals and departures of the EVs to/from the parking facility, we use an inhomogeneous continuous-time Markov chain (ICTMC)[20]. The process is inhomogeneous because the arrival and departure rates change over time. The state of the process represents the current size of the population and the transitions are limited to birth and death. Modeling the parking facility as an ICTMC captures the time dependency of the transition

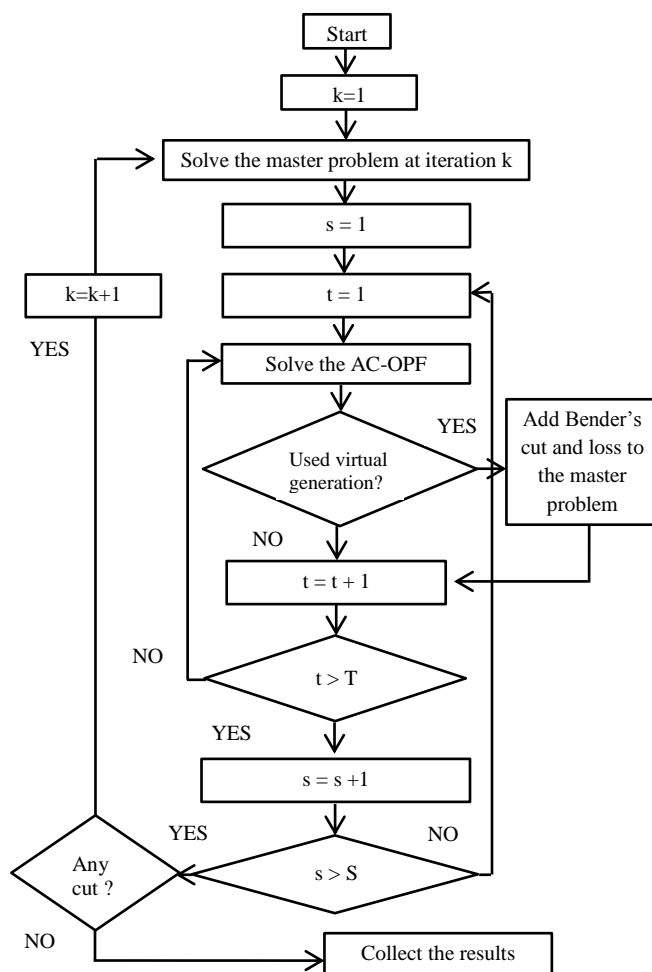


**Figure 2.2:** The solving algorithm's flow chart

rates. However, finding a closed-form solution for the transition probabilities is believed to be very difficult, if not impossible [20]. Several numerical methods have been proposed in the literature to solve the Kolmogorov forward equations numerically.

In this chapter, we use the Monte Carlo simulation to generate scenarios for the state transitions based on the ICTMC [20]. The state of the process is the number of parked EVs. The birth and death events are the arrivals and departures. We assume that an EV enters the parking at a rate  $\lambda(t)$  and leaves the parking at a rate  $i\mu(t)$  where  $i$  is the state of the system. Given the process is in state  $i$  at time  $t'$ , the holding time  $t$  is sampled from the

cumulative probability distribution function given in (2.30).

$$F_i(t|t') = 1 - \exp\left[-\int_{t'}^t (\lambda(t'') + i\mu(t''))dt''\right] \quad (2.30)$$

After determining the holding time  $t$ , the sampling of the next state  $j$ , is obtained by generating a random number  $U$  and selecting the state  $j$  that satisfies the constraint in (2.31). We continue sampling the holding times and jumps to the next states until we reach the end of the planning horizon (hour 24).

$$\sum_{k=0}^{j-1} q_{ik}(t) \leq U \leq \sum_{k=0}^j q_{ik}(t) \quad (2.31)$$

In (2.31),  $q_{ik}(t)$  is the conditional probability of transitioning to state  $k$  given that the current state is  $i$ . The value of  $q_{ik}(t)$  is given by (2.32).

$$q_{ik}(t) = \begin{cases} \lambda(t)/(\lambda(t) + i\mu(t)) & \text{if } i \leq k. \\ 0 & \text{if } i = k. \\ i\mu(t)/(\lambda(t) + i\mu(t)) & \text{if } i > k. \end{cases} \quad (2.32)$$

Notice that when the  $i$  equals the capacity of the parking facility,  $q_{ik}(t) = 1$  for  $i \leq k$ . We count the number of arrivals and departures during each hour  $(N_t^{arr}, N_t^{dep})$  which are used to compute according to (2.3) and (2.4) the maximum and minimum storage capacity  $(E_t^{max}$  and  $E_t^{min})$  at each hour. We generate scenarios for the values of  $(N_t^{arr}, N_t^{dep})$  by replicating the Monte Carlo simulation. After generating the scenarios, they are reduced by using the K-means clustering algorithm [24]. The number of scenarios is decreased to reduce the computational time of the solving algorithm.

## 2.7 Microgrid Description

### 2.7.1 Microgrid Topology

We run our experiments on a modified 14-bus microgrid test system introduced in [22]. The microgrid topology is shown in Figure 2.3. In the modified system, we add a 1 MW wind turbine at bus 1 and 1 MW solar panels at bus 4. We also aggregate all the EVs batteries in the parking facility as a single battery and replace the stationed load at bus 2 in [22] with the parking battery. The parking battery is connected to the battery side convertor and a transformer (13.8KV/2.4KV, 3.0 MVA) on the branch connecting bus 2 to the feeder. Three small scale thermal units are also added at bus 5, bus 10 and bus 12. The technical data related to the thermal units are summarized in Table 2.1.

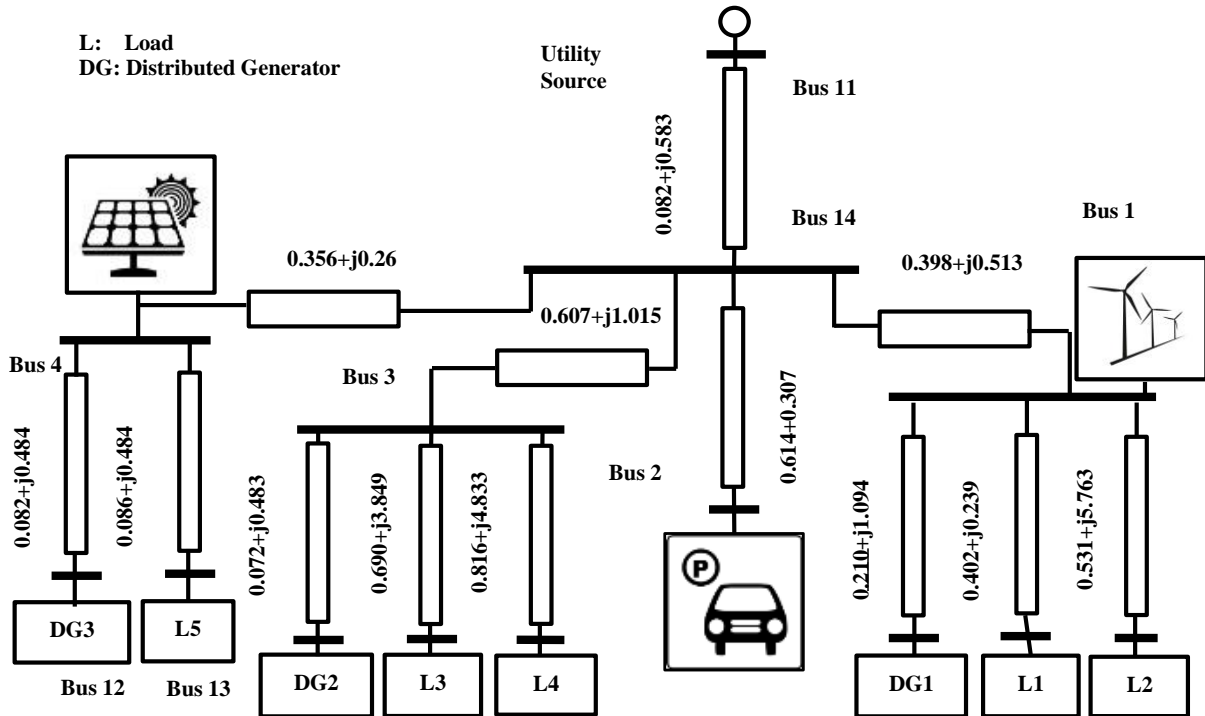


**Figure 2.3:** 14-bus microgrid test system

**Table 2.1:** Unit commitment technical data

Technical Parameter	1	2	3
Start up cost (\$)	200	250	220
Start up cost (\$)	150	180	160
Min up-time (hour)	3	3	3
Min down-time (hour)	2	2	2
Ramp up (MW/hr)	0.5	0.5	0.5
Ramp down (MW/hr)	0.5	0.5	0.5
Max capacity (MW)	1	1.5	1.1
Min capacity (MW)	0.1	0.2	0.1
Price of fuel(\$/Mft3)	10	10	10

### 2.7.2 EVs Parking Battery

We divide a typical day into four 6-hour intervals. The morning interval starts from 6am to noon with arrival rate  $\lambda_1$  and departure rate of  $\mu_1$ , the afternoon interval starts from noon to 6pm with arrival rate  $\lambda_2$  and departure rate of  $\mu_2$ , the evening interval starts from 6pm to midnight with arrival parameter  $\lambda_3$  and departure rate of  $\mu_3$ , and the night interval starts from 12am to 6am with arrival parameter  $\lambda_4$  and departure rate of  $\mu_4$ . The parking capacity is 200 EVs and  $\lambda_1, \lambda_2, \lambda_3, \lambda_4$  and  $\mu_1, \mu_2, \mu_3, \mu_4$  are 70, 60, 15, 10, and 0.33, 0.3, 0.5, 0.4, respectively. We generate 1000 scenarios for the number of vehicles in the parking facility according to the process described in Section V and reduce them to 10 scenarios using the K-means clustering algorithm described in [24]. In Figure 2.4, we show three of these scenarios. The battery capacity of an EV is 0.04 MWh and the average arrival energy content, SOC, is 50%.

The rated capacity of the chargers  $CH^{max}$  is 0.02 MWh. The maximum and minimum allowed SOC of an EV's battery is 0.9 and 0.1, respectively. The cost of battery wear,  $\gamma$ , is assumed to be 10 (\$/MWh).

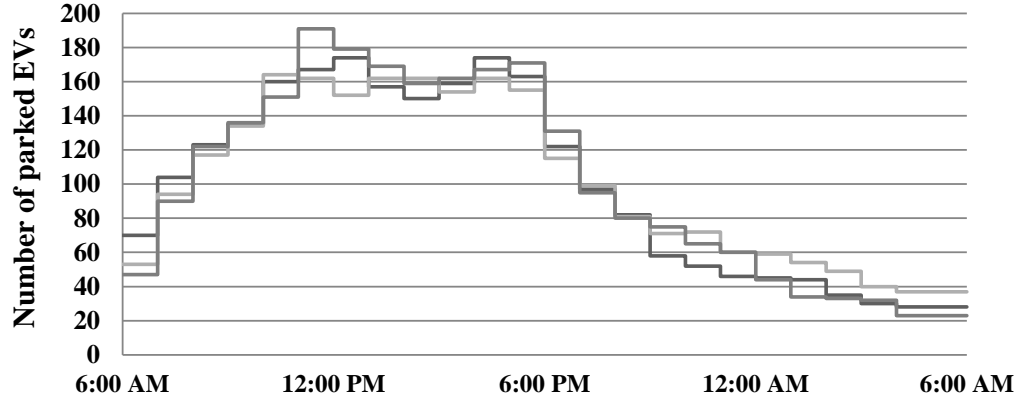


**Figure 2.4:** The scenario sample for the number of parked EVs.

### 2.7.3 Day-ahead energy prices and power distributor

The energy prices on June 11, 2013 from [23] are assumed to be the forecasted prices. They are given in Figure 2.5. For the real-time transactions, the microgrid imports energy at a cost of 850 (\$/MWh) and exports it at a price of 150 (\$/MWh).

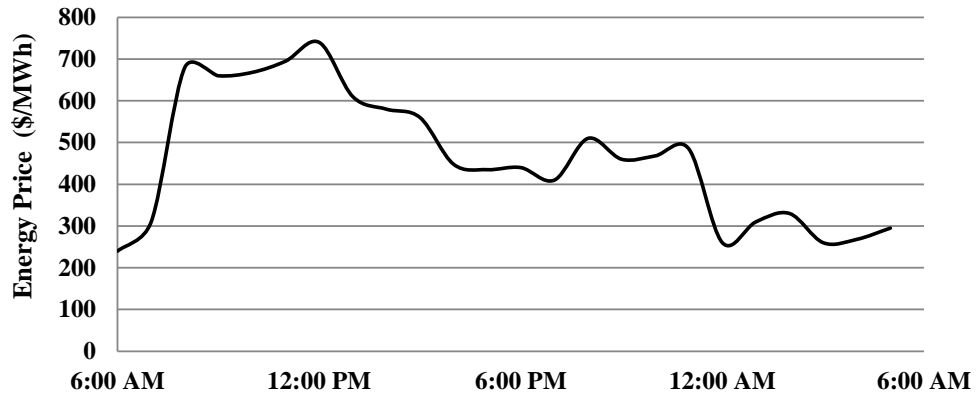


**Figure 2.5:** Energy price in the day-ahead.

### 2.7.4 Net Demand Uncertainty

The Monte Carlo simulation is used to generate scenarios for representing the uncertainties in demand, wind energy and solar energy. As the solar and wind energy sources are assumed to be non-dispatchable, the net demand scenarios at each hour are obtained by subtracting the wind and solar energy output from the demand at that hour. To generate the scenarios, we use a truncated multivariate normal distribution (TMVN) [24]. The probability density function of TMVN is given in (22) [25]. The covariance matrix,  $\Sigma$ , represents the between hour interdependency.

$$f(x, \mu, \Sigma, a, b) = \frac{\exp(-1/2(x - \mu)^T \Sigma^{-1} (x - \mu))}{\int_a^b \exp(-1/2(x - \mu)^T \Sigma^{-1} (x - \mu)) dx} \quad (2.33)$$

To estimate the parameters of the TMVN, we use wind and solar energy output data provided by the renewables integration study datasets in [26]. We also collected historical hourly demand data from [23]. We generate 100,000 net demand scenarios for 24 hours and reduced them to 10 scenarios using the K-means clustering algorithm. In Figure 2.6, we show a sample of three of these scenarios.

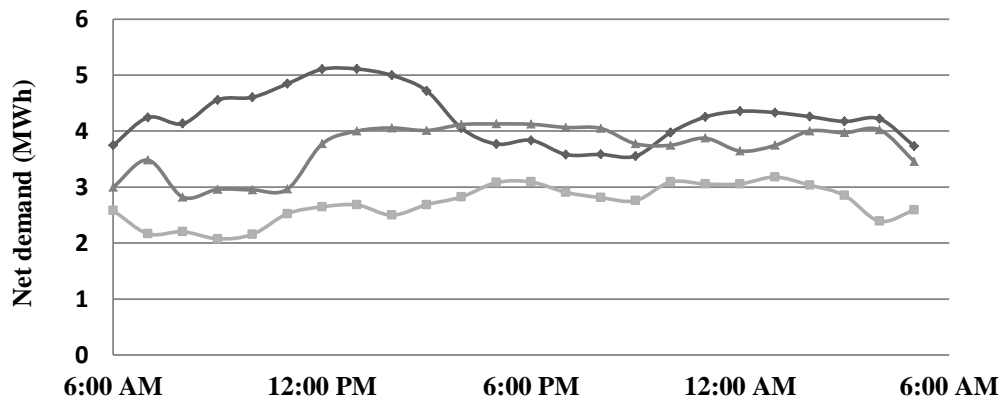


**Figure 2.6:** Sample of net load scenarios

## 2.8 Simulation Results

We run all of the simulations on a 2.8 GHz Core 2Duo processor with 4GB of memory. The results are used to assess the effects of the parking facility, parking time, departure policies and net load and parking uncertainties. As we consider 10 scenarios for the net load and 10 scenarios for the parked EVs, the problem is solved for 100 scenarios based on all combinations. It takes 1h 56mins for the Benders' decomposition to converge after 50 iterations. In Table 2.2, we show the purchases/sales in the day-ahead market. The expected total operation cost (ETOC) is \$28,545 and all thermal units are committed during the operation day.

**Table 2.2:** Purchases/sales in the day ahead

$x_t(\text{MWh})$							
6am	7am	8am	9am	10am	11am	12pm	1pm
3.6	3.27	1.83	1.8	0.36	1.4	3.15	0.81
2pm	3pm	4pm	5pm	6pm	7pm	8pm	9pm
0.42	0.98	1.03	3.96	0.33	3.01	1.29	1.38
10pm	11pm	12am	1am	2am	3am	4am	5am
0.33	0.51	4.23	2.22	1.29	3.15	2.70	1.29

Table 2.3 gives the hourly maximum, minimum and average charged/discharged energy to/from the parking battery over all scenarios in the operation day. These results show that the parking battery is either charged or remains unused at 3am, 6am and 9pm, and is certainly charged at 7am, 5pm, 7pm and 12am due to the low price of energy at those hours. At 8am, 11am, 12pm, 6pm, 8pm, 10pm, 11pm and 5am, the parking battery is either discharged or remains unused and at 2am the battery is certainly discharged due to the high price of energy at those hours. For the remaining hours, the parking battery is either charged or discharged based on a particular scenario.

**Table 2.3:** Charging/discharging of the parking battery

	$y_t(\text{MWh})$							
	6am	7am	8am	9am	10am	11am	12pm	1pm
Max	1.13	1.24	0.00	1.81	0.43	0.00	0.00	0.92
Min	0.00	0.41	3.05	0.93	2.61	2.35	2.24	1.88
Mean	0.78	0.66	1.02	0.82	0.32	0.79	1.97	0.00
	2pm	3pm	4pm	5pm	6pm	7pm	8pm	9pm
Max	0.55	0.34	0.68	3.26	0.00	2.30	0.00	1.33
Min	1.39	2.05	0.47	1.47	2.22	0.93	1.92	0.00
Mean	0.11	0.19	0.09	2.57	1.01	1.87	2.05	0.81
	10pm	11pm	12am	1am	2am	3am	4am	5am
Max	0.00	0.00	0.93	0.23	0.24	0.74	0.45	0.00
Min	1.24	1.12	0.03	0.48	0.86	0.00	0.14	0.76
Mean	0.86	0.62	0.66	0.23	0.62	0.27	0.06	0.41

### 2.8.1 Effect of using the parking facility

To show the effect of the parking facility on the microgrid, we solve the model without the parking facility. We set the number of available EVs to zero to simulate that no parking facility exists. As in the case we have the parking facility, all thermal units are committed during the operation day. The ETOC with no parking facility is \$31,106, which is \$2,561 higher than using it. The purchases/sales in the day-ahead market are given in Table 2.4. Without parking facility, the microgrid does not have any storage capacity, and thereby it has to purchase energy from the day-ahead market at prevailing price.

**Table 2.4:** Purchases/sales in the day ahead

	$x_t(\text{MWh})$							
	6am	7am	8am	9am	10am	11am	12pm	1pm
	3.12	2.44	0.33	0.11	0.12	0.21	0.49	0.93
	2pm	3pm	4pm	5pm	6pm	7pm	8pm	9pm
	0.81	0.86	0.81	1.03	0.82	0.91	0.59	0.67
	10pm	11pm	12am	1am	2am	3am	4am	5am
	0.69	1.37	3.36	1.99	1.86	2.33	2.63	1.91

## 2.8.2 The value of considering uncertainty

As we have considered the uncertainty of the net load and the number of parked EVs, we assess the individual and combined effects of these two uncertainty sources. To assess the individual effects, we solve the problem considering one scenario for one parameter and 10 scenarios for the other. The one scenario is obtained by averaging the 10 scenarios of each parameter. For instance, to compute the value of considering the net load uncertainty, we solve the model using one scenario for the net load and 10 scenarios for the parked EVs. The ETOC of the solved problem is \$31,794 which is \$3,249 higher than that of the stochastic problem with 100 scenarios. Similarly, to compute the value of considering the parked EVs' uncertainty, we solve the model with one scenario for the parked EVs and 10 scenarios for the net load. The ETOC of the solved problem is \$30,746 which is \$2,201 higher than that of the stochastic problem with 100 scenarios. For the combined effect, we use one net load and parked EVs scenario. The ETOC of the solved problem is \$34,179, which is \$5,634 higher than the stochastic model with 100 scenarios. The purchases/sales in the day-ahead market are given in Table 2.5. The ETOC is calculated by determining the first stage decision variables and then using them to obtain the second stage decisions for each of the 100 scenarios. The ETOC is obtained by averaging the operation costs of each scenario.

**Table 2.5:** Purchases/sales in the day ahead

$x_t(\text{MWh})$							
6am	7am	8am	9am	10am	11am	12pm	1pm
4.37	4.27	1.77	3.98	1.76	0.32	1.06	2.11
2pm	3pm	4pm	5pm	6pm	7pm	8pm	9pm
1.81	1.35	1.98	5.20	0.92	3.41	0.08	2.33
10pm	11pm	12am	1am	2am	3am	4am	5am
1.23	1.36	5.95	2.17	1.82	4.52	2.12	1.26

### 2.8.3 Effect of battery wear cost

To evaluate the effect of battery wear cost on the EVs' charging/discharging amounts and the expected cost savings, we solve the model with different values for  $\gamma$ . The results have been summarized in Table 2.6. We computed the hourly charging/discharging amounts at each case by averaging the EV's charging or discharging values over all scenarios and dividing the obtained number by 24. As  $\gamma$  decreases, the cost of battery wear decreases and the microgrid discharges the EVs' batteries deeper. Clearly, the expected cost savings is higher for lower  $\gamma$  values. However, lowering the value of  $\gamma$  can reduce the EV owners motivation for participating in the V2G program.

**Table 2.6:** Effect of battery wear cost

$\gamma$ (\$/MWh)	Average hourly charging /discharging (MWh)	Hourly cost of battery wear (\$)	Expected cost savings (\$)
2	1.48	2.96	2,864
4	1.42	5.68	2,804
6	1.36	8.16	2,739
8	1.28	10.24	2,666
10	1.20	12.00	2,561
12	1.02	12.24	2,509
14	0.86	12.04	2,416
16	0.71	11.36	2,329
18	0.52	9.36	2,246
20	0.29	5.80	2,073

### 2.8.4 Effect of the EVs parking time on expected cost savings

To evaluate the effect of the EVs' parking time, we solve the model considering different values of  $\mu$ . The expected cost savings are computed in comparison to the case where the parking facility is not used for energy storage. Fig. 2.7 shows the impact of the expected parking time ( $1/\mu$ ) on the microgrid's expected cost savings. Clearly, as the expected parking time increases, the expected cost savings increase. The contribution of the parking facility

becomes more significant as the vehicles are available to the microgrid for longer hours. Note that the capacity of the parking facility restricts the expected cost savings to \$3600.

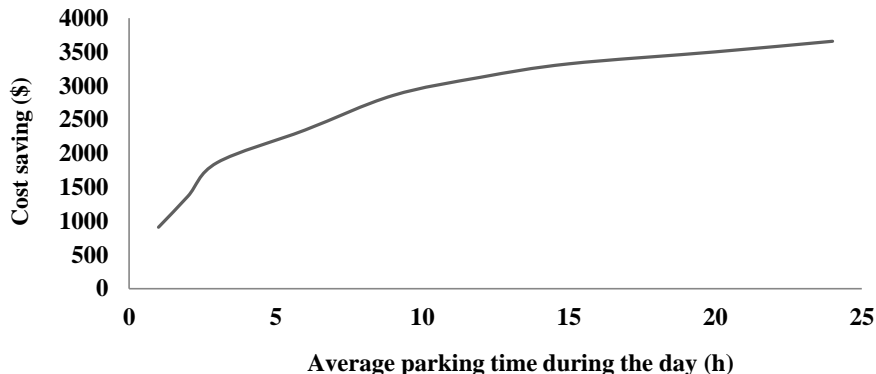


**Figure 2.7:** The effect of parking time on the expected cost savings

### 2.8.5 Effect of arrival and departure rates

The benefits of the EVs' integration into the microgrid depend on the arrival and departure rates. In Table 2.7, we show the different arrival rates of three different cases during a day. For Case 1, 2, and 3, we use as departure rate ( $\mu$ ) the values 0.5, 0.33, and 0.2, respectively. Notice that these three cases represent short-, medium-, and long- time parking behaviors. The expected cost savings for Case 1, 2, and 3 are \$243, \$409, and \$537, respectively. Notice that the expected cost savings in case 3 are relatively higher than those in cases 1 and 2 because the average parking time of the EVs is longer.

### 2.8.6 Effect of market price fluctuations

To assess the effect of market price fluctuations on expected cost savings, we modify the forecasted market prices (shown in Figure 2.5) to create different fluctuation ratios. The fluctuation ratio is calculated by dividing the highest energy price by the lowest price during the operation day. The fluctuation ratio of the forecasted prices is 3.5. The expected cost savings for different fluctuation ratios are shown in Table 2.8. The table also shows the

**Table 2.7:** Arrival Rates ( $\lambda$ ) for different cases at each hour

Time	6am	7am	8am	9am	10am	11am	12pm	1pm
Case 1	60	60	40	40	50	50	30	30
Case 2	60	60	60	60	20	20	20	20
Case 3	60	60	60	60	20	20	20	20
Time	2pm	3pm	4pm	5pm	6pm	7pm	8pm	9pm
Case 1	40	40	40	30	30	30	20	20
Case 2	40	40	40	40	20	20	20	20
Case 3	40	40	40	40	20	20	20	20
Time	10pm	11pm	12am	1am	2am	3am	4am	5am
Case 1	20	10	10	10	5	5	5	5
Case 2	20	10	10	10	10	5	5	5
Case 3	20	10	10	10	10	5	5	5

percentage of increase or decrease in the savings compared to the savings of the original forecasted prices. Clearly, higher price fluctuations generate higher expected cost savings.

**Table 2.8:** Microgrid’s cost savings under different fluctuation rates

Fluctuation rate	Expected cost saving (\$)	Increase/decrease (%) compared to 3.5 rate
1	0	-100%
1.5	706	-72%
2	1,104	-57%
2.5	1,652	-35%
3	2,113	-17%
3.5	2,561	0%
4	3,111	21%
4.5	3,598	40%
5	3,996	56%

### 2.8.7 Interaction effect of market price fluctuations and EVs’ arrival and departure rates

We define five hypothetical fluctuation profiles “A to E”, given in Table 2.9, for the day-ahead market prices and use the EV’s arrival and departure rates defined in Table 2.7 to assess the interaction effect. Profiles A and B represent high fluctuation ratios, C no

price fluctuation, and D and E low fluctuation ratios. The expected cost savings under these different conditions are summarized in Table Table 2.10. The expected savings under no price fluctuation (profile C) are zero, regardless of the arrival and departure rates. In case 1, the higher expected cost savings are obtained under price profiles A and D. The reason is that in case 1 the arrivals exceed the departures during high price hours. The microgrid operator can discharge the arriving EVs at high price arrival hour and return the borrowed energy when the price is low. However, under profiles B and E, the arriving EVs should not be discharged at their arrival hour because the borrowed energy would need to be returned at a high price hour. Case 1 under profiles B and D illustrates the interaction effect between price fluctuations and EV’s arrival and departure rates. Although under profile B the price fluctuation ratio is higher than profile D, the expected savings under profile D are higher than under profile B. Similarly, cases 2 and 3 illustrate the interaction effect.

**Table 2.9:** Hypothetical patterns for day ahead market prices (\$/MWh)

Price profile	6am	7am	8am	9am	10am	11am	12pm	1pm
A	800	800	200	200	800	800	200	200
B	800	800	800	800	200	200	200	200
C	500	500	500	500	500	500	500	500
D	500	500	200	200	500	500	200	200
E	500	500	500	500	200	200	200	200
Price profile	2pm	3pm	4pm	5pm	6pm	7pm	8pm	9pm
A	800	800	800	200	200	200	800	800
B	800	800	800	800	200	200	200	200
C	500	500	500	500	500	500	500	500
D	500	500	500	200	200	200	500	500
E	500	500	500	500	200	200	200	200
Price profile	10pm	11pm	12am	1am	2am	3am	4am	5am
A	800	200	200	200	200	200	200	200
B	200	800	800	800	800	200	200	200
C	500	500	500	500	500	500	500	500
D	500	200	200	200	200	200	200	200
E	200	500	500	500	500	200	200	200

**Table 2.10:** Cost savings under different price profiles and arrivals/departures.

	A	B	C	D	E
Case 1	\$352	\$102	\$0	\$156	\$73
Case 2	\$330	\$583	\$0	\$134	\$291
Case 3	\$419	\$684	\$0	\$197	\$374

### 2.8.8 Effect of restricting the departures

Enforcing some restrictions on departures can increase the expected cost savings. Any restriction should be compensated so that there is enough motivation for the EV owners to participate in the restricted program. In the restricted program, the participating EVs are not allowed to depart the parking facility in certain hours. In our simulation, we use the arrival rates given in Section 5 and assume that the EVs can depart at predetermined time windows (9am to 10am, 5pm to 6pm or 11pm to 12am). The expected cost savings is \$3,084, representing a 20% increase compared to that of the case without restriction. The expected cost savings for SOC=0.1 is \$2,996 (16% increase) and for SOC=0.9 is \$3,178 (24% increase). As the microgrid controls the departures, a higher SOC produces higher expected savings. The microgrid can discharge the batteries of the EVs during high price hours and return the borrowed energy during low price hours. The time windows can be determined by the microgrid operator and can be based on the market price forecasting and mutual contracts between the microgrid and the customers.

## 2.9 Conclusions

We proposed to use the batteries of EVs in a parking facility for energy storage within a microgrid. We developed a two-stage stochastic model for managing the energy in a grid-connected microgrid that includes different sources of energy generation and a parking facility for the EVs. We used an inhomogeneous continuous time Markov chain to model the variable capacity of the parking facility. We simulated the proposed model on a 14-bus distribution test system and solved it using the Benders' decomposition method. The simulation results

showed that using the EVs' batteries reduces the cost of the electricity generation. We also assessed the effects on expected cost savings caused by uncertainty, expected parking time, market price fluctuations, SOC and arrival and departure rates. The results showed that longer parking times and higher price fluctuation ratios produce higher expected savings. Also, the interaction effect of price fluctuation ratios and EV's parking behavior can have a significant impact on expected savings. That is, having a high price fluctuation ratio does not necessarily mean high expected savings. By considering the interaction effect of price fluctuation and EVs' parking behavior, we designed a restricted mechanism for the parking facility to improve the benefits. The results from the restricted program confirmed the positive contribution on the expected cost savings. The results also showed the superiority of the stochastic model compared to the deterministic one.

## References

- [1] X. Fang, S. Mishra, G. Xue and D. Yang, “Smart Grid The New and Improved Power Grid: A Survey”, *Communications Surveys and Tutorials, IEEE*, vol. 14, no. 4, pp. 944-980, 2012.
- [2] Z. Huang, T. Zhu, Y. Gu, D. Irwin, A. Mishra and P. Shenoy, “ Minimizing electricity costs by sharing energy in sustainable microgrids ”, *In Proceedings of the 1st ACM Conference on Embedded Systems for Energy-Efficient Buildings* 2014.
- [3] J. A. Lopes, F. J. Soares and P. M. Almeida, “Integration of electric vehicles in the electric power system”, *In Proceedings of the IEEE*, 2011.
- [4] M. Gonzalez Vay and G. Andersson, “Centralized and decentralized approaches to smart charging of plug-in vehicles”, *textit IEEE in In Power and Energy Society General Meeting*, 2012.
- [5] M. Gonzalez Vaya and G. Andersson, “Optimal bidding strategy of a plug-in electric vehicle aggregator in day-ahead electricity markets under uncertainty”, *IEEE Transactions on Power Systems*, vol. 99, pp. 1-11, 2014.
- [6] D. Wu, D. C. Aliprantis and L. Ying, “Load scheduling and dispatch for aggregators of plug-in electric vehicles”, *IEEE Transactions on Smart Grid*, vol. 3, no. 1, pp. 368-376, 2012.
- [7] C. Jin, J. Tang and P. Ghosh, “Optimizing electric vehicle charging with energy storage in the electricity market”, *IEEE Transactions on Smart Grid*, vol. 4, no. 1, pp. 311-320, 2013.

- [8] S. Derakhshandeh, A. Masoum, S. Deilami and M. Hamedani Golshan, "Coordination of generation scheduling with PEVs charging in industrial microgrids", *IEEE Transactions on Power Systems*, vol. 28, no. 3, pp. 3451-3461, 2013.
- [9] J. Van Roy, N. Leemput, F. Geth, J. Buscher, R. Salenbien and J. Driesen, "Electric vehicle charging in an office building microgrid with distributed energy resources", *IEEE Transactions on Sustainable Energy* vol. 5, no. 4, pp. 1389-1396, 2014.
- [10] U. Chukwu and S. M. Mahajan, "V2G parking lot with pv rooftop for capacity enhancement of a distribution system", *IEEE Transactions on Sustainable Energy*, vol. 5, no. 1, pp. 119-127, 2014.
- [11] T. Wu, Q. Yang, Z. Bao and W. Yan, "Coordinated energy dispatching in microgrid with wind power generation and plug-in electric vehicles", *IEEE Transactions on Smart Grid* vol. 4, no. 3, pp. 1453-1463, 2013.
- [12] C. Chen and S. Duan, "Optimal integration of plug-in hybrid electric vehicles in microgrids" , *IEEE Transactions on Industrial Informatics*, vol. 10, no. 3, pp. 1917-1926, 2014.
- [13] W. Su, J. Wang and J. Roh, "Stochastic energy scheduling in microgrids with intermittent renewable energy resources", *IEEE Transactions Smart Grid* vol. 5, no. 4, pp. 1876-1883, 2014.
- [14] D. Nguyen and L. Le, "Optimal energy trading for building microgrid with electric vehicles and renewable energy resources", *In Innovative Smart Grid Technologies Conference, IEEE*, 2014.
- [15] Y. Feng and S. Ryan, "Scenario reduction for stochastic unit commitment with wind penetration", *PES General Meeting, Conference and Exposition* 2014.

- [16] H. Khodr, J. Martinez-Crespo, M. Matos and J. Pereira, "Distribution systems reconfiguration based on OPF using Benders decomposition," *IEEE Transactions on Power Delivery*, vol. 24, no. 4, pp. 2166-2176, 2009.
- [17] M. Shahidehpour, F. Yong, "Benders' decomposition in restructured power systems", *IEEE Techtorial*, April 2005.
- [18] M. Gay, "IBM ILOG CPLEX Optimization Studio CPLEX User's Manual", vol. 12, International Business Machines Corporation, 2012.
- [19] R. D. Zimmerman, C. Murillo-Sanchez and R. Thomas, "Matpower: Steady-State Operations, Planning and Analysis Tools for Power Systems Research and Education", *IEEE Transactions on Power Systems*, vol. 26, no. 1, pp. 12-19, 2011.
- [20] L. Y.F., L. Y.H. and Z. E., "Sochastic modeling by inhomogeneous continuous Markov chain", *URO Workshop on Stochastic Modeling*, May 2012.
- [21] L. Baringo and A. Conejo, "Correlated wind-power production and electric load scenarios for investment decisions", *Applied Energy*, vol. 101, pp. 475-482, 2013.
- [22] F. Katiraei and M. Iravani, "Power management strategies for a microgrid with multiple distributed generation units", *IEEE Transactions on Power Systems*, vol. 21, no. 4, pp. 1821-1831, 2006.
- [23] PJM, "Operational Analysis ", 2014. [Online]. Available: <http://www.pjm.com>.
- [24] P. Pinson, G. Papaefthymiou, B. Klockl and H. Nielsen, "From probabilistic forecasts to statistical scenarios of short-term wind power production", *Wind energy*, vol. 12, no. 1, pp. 51-62, 2009.
- [25] S. Wilhelm and B. Manjunath, "tmvtnorm: A package for the truncated multivariate normal distribution," *sigma 2*, vol. 2, 2010.

- [26] NREL, “The Dynamic Maps, GIS data and Analysis Tools”, 2014. [Online]. Available:  
*[http : //www.nrel.gov/gis/data\\_ind.html](http://www.nrel.gov/gis/data_ind.html)*.

## Chapter 3

### Optimal Investment to Upgrade a Microgrid Parking Facility with V2G Technology

#### 3.1 Abstract

Microgrids are usually powered by small scale distributed generators, renewable energy resources and batteries. The batteries of the electric vehicles (EVs) in the parking facility can be managed to store energy and power the microgrid. We propose a mathematical investment model to upgrade the parking facility of a microgrid with V2G technology to increase energy storage capacity. The model aims to determine the optimal number of V2G stations in the parking facility by minimizing the sum of the investment and operation costs. The former is the required capital investment for the purchase of the V2G stations, and the latter is the cost of generation dispatch to meet the demand at each hour. The uncertainty of the demand and the EVs arrivals and departures and the intermittency of the renewable resources are all taken into account. We use the Benders' decomposition to compute the cost of generation dispatch and the Nelder-Mead algorithm to search for the optimal number of V2G stations. Numerical experiments are conducted on a 14-bus microgrid test system for a planning horizon of five years. The results show that investing in the V2G technology increases the long-term economics of the microgrid.

**Keywords:** Microgrid, Electric Vehicle, V2G Investment, Nelder-Mead algorithm

#### 3.2 Introduction

Due to major advancements in smart grid and rapid expansion of renewable resources, investing on energy storage technologies has become very important. Batteries of electric vehicles (EVs) have been proposed as a cost-effective alternative to large scale grid energy

storage [1]. In addition to energy storage, the EVs can provide the grid with peak shaving [1], system stability [2], voltage and frequency regulations [3], emission reduction [4], or other economic benefits [5] in the charging/discharging [6] or charging-only [7] modes. They can also be integrated into the distribution grid [8], the microgrids [9] or the aggregator entities [10] and charged or discharged under centralized or decentralized [11] schemes. The optimal siting and sizing of EV charging stations has been studied in [12]. The model considered the road networks and potential locations for the stations but ignored all of the operational constraints and energy market interactions. A similar problem has been studied in [13] where the optimal decisions were made within the boundaries of the distribution grid. In [8], the long-term integration of EVs into a microgrid was discussed. The study did not consider the interactions with energy markets, the inherent uncertainties, and the dispatch of generation. In [14], the optimal siting and sizing of distributed generation with a parking facility was modeled. The power losses were minimized in the distribution grid but the economic aspects were not taken into account. The size of the parking facility was assumed to be fixed.

To provide additional energy and storage, we have proposed in [15] a framework that integrates EVs into a microgrid. We formulated an optimization model that minimizes the expected total operation costs and solved it using the Benders decomposition algorithm. The grid-connected microgrid included small scale thermal units, renewable energy resources and a parking facility for EVs. The number of V2G stations in the parking facility was assumed to be known. In this chapter, we propose an optimization model to obtain the number of V2G stations by minimizing the total cost of the microgrid. The total cost consists of the investment and operation costs. The former is the required capital investment for one-time purchase of the V2G stations at the beginning of the planning horizon. The latter is the cost of energy dispatch to meet the demand at each hour which includes the cost of generation, purchases/sales in the day-ahead market and battery wear. As our model involves uncertainty, a two stage stochastic programming framework is used to model the problem. The first stage decisions are made according to the available data in the first stage

and the recourse actions are taken in the second stage after the uncertain data are revealed. In the model, the first stage costs include investment costs, hourly commitment costs of the thermal units and the purchases/sales in the day-ahead market. The second stage costs are the expected costs of generation, battery wear and real-time balancing. The available EVs in the parking facility and the output of the renewable resources are the uncertain parameters.

Finding the optimal number of V2G stations in the parking facility is challenging because we need to solve the proposed stochastic problem at each hour for a long planning horizon. Moreover, considering uncertainty, unit commitment and power flow constraints make the solving algorithm computationally expensive. We use the Nelder-Mead heuristic algorithm [16] together with Benders' decomposition [19] to solve the optimization problem. The Nelder-Mead algorithm searches for the optimal number of V2G stations in the parking facility by minimizing the total cost. The total cost is computed by decomposing the problem into two sub-problems: operation and investment. The investment cost is computed by the Nelder-Mead and operation cost is computed by the Benders' decomposition.

The remainder of this chapter is organized as follows: in Section 3.3, the optimization model is described. Section 3.4 gives the mathematical formulation. Section 3.5 presents the solving algorithm, and Section 3.6 explains the stochastic modeling of the parking facility. In section 3.7, the microgrid's test system is discussed and in section 3.8, the numerical results are provided. Section 3.9 draws the conclusions.

### **3.3 Problem Description**

Similar to the considered microgrid in chapter 2, in this chapter, we assume a microgrid consisting of conventional thermal units, small-scale wind turbines, solar panels and an EV parking facility. It is also assumed that the microgrid operates in a grid-connected mode and purchase/sells energy in the day-ahead market. To resolve the imbalances between the predicted and actual demand and supply, the microgrid operator agrees with a local power distributor to exchange excess supply or demand for fixed predefined prices. An agreement

with a local distributor at a fixed price can hedge against the highly volatile prices of the real-time market.

### **3.3.1 Parking facility for energy storage**

To use the parking facility as an energy and storage resource, the parking stalls should be equipped with V2G stations. The two-way electric flow capability provided by the V2G stations enables the microgrid operator to store or withdraw energy in/from the batteries of the available EVs in the parking. The energy storage ability allows the microgrid to shift the energy purchases from high-price to low-price hours and inversely energy sales from low-price to high-price hours. The capacity of the supplied energy storage depends on the number of V2G stations and the number of available EVs in the parking facility.

### **3.3.2 Modeling Uncertainty**

The proposed model is formulated as a two stage stochastic optimization problem. In the first stage, the price of energy in the day-ahead market is forecasted and the contracted prices with the power distributor are assumed to be known. The number of V2G stations, commitment schedule of the thermal units, and the energy purchases/sales in the day-ahead market are also determined. The net demand and the capacity of the parking facility are modeled as stochastic parameters. To represent the uncertainty on these parameters, we generate scenarios. The second stage ensures that the power balance constraint is satisfied for each scenario.

## **3.4 Problem Formulation**

The formulation of the investment model includes the objective function and system constraints.

### 3.4.1 Objective Function

The objective function is given in (3.1) and minimizes the present worth of the expected total costs of the microgrid. The total cost includes the costs of first stage decisions and the expected cost of the second stage decisions over all scenarios. The first stage costs are the one-time V2G investment cost, hourly cost of energy purchases and sales in the day-ahead market and hourly startup and shutdown costs of the thermal units over the planning horizon. The second stage costs are the hourly generation cost of the thermal units, cost of battery wear and the cost of power exchanges (balancing) with the local power distributor at each scenario  $s$ .

$$Min z = \vartheta n + \sum_{yr=1}^{YR} 1/r \left[ \sum_t (P_t^{da} x_t) + \sum_t \sum_j (s_{jt}^{up} + s_{jt}^{sd}) + \sum_t \sum_s \pi_s \sum_j (c_j^f f_{jt,s} + \gamma(y_{t,s}^+ + y_{t,s}^-) + \varphi z_{t,s}) \right] \quad (3.1)$$

### 3.4.2 Constraints

We consider all Constraints (2.1) - (2.27) for this problem as well. In addition, we introduce two new capacity Constraints (3.2) and (3.3) for the parking battery. Constraints in (3.2) and (3.3) restrict the maximum and minimum capacity of the parking battery to the number of V2G stations.

$$E_{t,s}^{min} = E^{min}(n\beta) \quad \forall t, \forall s \quad (3.2)$$

$$E_{t,s}^{max} = E^{max}(n\beta) \quad \forall t, \forall s \quad (3.3)$$

### 3.5 Solving Algorithm

As noted earlier, solving the model (3.1)-(3.3) considering all constraints (2.1) - (2.27) is extremely difficult. To overcome this difficulty, we split the optimization into two sub

problems: investment and operation. The investment problem determines the capital cost of purchasing  $n$  V2G stations, and the operation problem determines the cost of operating the microgrid with  $n$  stations. The operation cost is computed by solving the model without constraints (3.2) and (3.3) and no investment term in the objective function (3.1).

### 3.5.1 Finding the optimal value of $n$

To search for the optimal value of  $n$ , we use the Nelder-Mead heuristic algorithm [16]. The algorithm is a derivative-free search method for multidimensional unconstrained optimization problems [18]. It has been proved that for a function with one dimension the Nelder-Mead algorithm always converges to an optimal solution [16]. In our case, the function to be minimized  $f(n)$  is the required investment on purchasing  $n$  V2G stations plus the operation cost considering there are  $n$  stations in the parking facility. The five steps of the algorithm (reorder, reflect, expand, contract and shrink) are shown in Figure 3.1.

### 3.5.2 Computing the operation cost

Solving the operation problem for the entire planning horizon is computationally intractable. Therefore, we divide the planning horizon into shorter intervals using the approach given in [17]. This approach associates the variability of demand, wind and solar power to meteorological fluctuation of seasons, days and hours. A similar approach is used to represent the variability of the EVs arrivals and departures to/from the parking facility. As there are four different seasons within a year, we use four representative weeks. The operation problem is then solved separately for each week (168 consecutive hours). The four values of the objective function are multiplied by the number of weeks within each season to obtain the operation cost for the entire year. The procedure is repeated for the other years of the planning horizon.

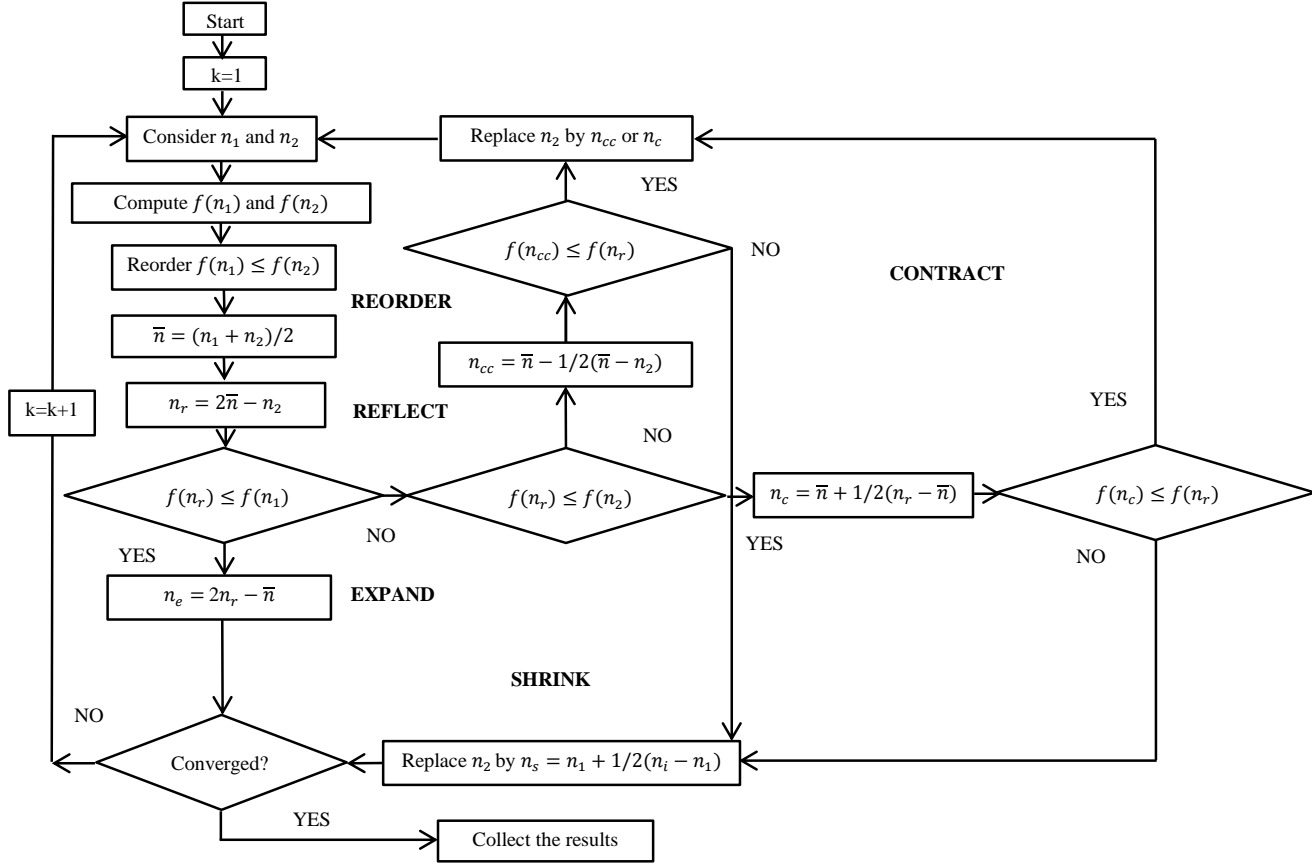


**Figure 3.1:** Nelder-Mead algorithm

To solve the model for weekly intervals, we use the Benders' decomposition method [19]. We partition the problem into two problems: a master problem and a sub-problem. The master problem includes the entire operation problem without the AC-OPF constraints (14) to (18). The sub-problem includes the AC-OPF constraints. To solve the master problem, we use the IBM ILOG CPLEX interactive optimizer with Concert technology in C++ [20]. We use Matpower 5.1 [21] to solve the sub-problem. The Benders' decomposition with details has been discussed in [15].

### 3.6 Stochastic modeling of the parking facility

Similar to Section (2.4.4), we model the arrivals and departures of the EVs to/from the parking facility using an Inhomogeneous Continuous Time Markov Chain (ICTMC) [22, 23] and use the Monte Carlo simulation to generate scenarios for the state transitions based on the ICTMC. The holding time is sampled from the cumulative probability distribution function given in (2.30). After determining the holding time, the sampling of the next state, is obtained by generating a random number and selecting the new state that satisfies the constraint in (2.31). We continue sampling the holding times and jumps to the next states until we reach the end of the planning horizon (hour 168).

Note that when the current state equals  $n$  in (2.32), the capacity of the parking facility,  $q_{ik}(t) = 1$  for  $i \leq k$ . We count the number of arrivals and departures during each hour ( $N_t^{arr}$  and  $N_t^{dep}$ ) which are used to compute the maximum and minimum storage capacity ( $E_t^{max}$  and  $E_t^{min}$ ) at each hour. We generate scenarios for the values of  $N_t^{arr}$  and  $N_t^{dep}$  by replicating the Monte Carlo simulation. The generated scenarios are reduced by using the K-means clustering algorithm to decrease the computational time [24].

### 3.7 Microgrid Description

#### 3.7.1 Microgrid Topology

We run our experiments on the 14-bus modified shown in Figure 2.3. We add a 1 MW wind turbine at bus 1, 1 MW solar panels at bus 4 and EVs' batteries at bus 2. Three small scale thermal units are also added at bus 5, bus 10 and bus 12. The technical data related to the thermal units are the same as the ones given in Table 2.1.

#### 3.7.2 EVs Parking Battery

We divide a typical day into four 6-hour intervals. The morning interval starts from 6am to noon with arrival rate  $\lambda_1$  and departure rate of  $\mu_1$ , the afternoon interval starts from

noon to 6pm with arrival rate  $\lambda_2$  and departure rate of  $\mu_2$ , the evening interval starts from 6pm to midnight with arrival parameter  $\lambda_3$  and departure rate of  $\mu_3$ , and the night interval starts from 12am to 6am with arrival parameter  $\lambda_4$  and departure rate of  $\mu_4$ . The remaining EVs during the last hour of the night interval are the available EVs for the starting hour of the morning interval of the next day. The arrival and departure rates for a week in spring have been summarized in Table 3.1. One scenario for the available number of EVs in a parking facility with 200 EVs during one week in spring is given in Figure 3.2.

**Table 3.1:** Arrival and departure rates for a week in spring

Day	Arrival rates				Departure rates			
	$\lambda_1$	$\lambda_2$	$\lambda_3$	$\lambda_4$	$\mu_1$	$\mu_2$	$\mu_3$	$\mu_4$
Monday	70	60	15	10	0.33	0.30	0.50	0.40
Tuesday	80	75	20	15	0.30	0.30	0.55	0.42
Wednesday	75	70	15	10	0.33	0.30	0.50	.45
Thursday	70	65	20	12	0.32	0.33	0.60	0.40
Friday	75	70	20	15	0.30	0.33	0.50	0.45
Saturday	45	40	10	5	0.40	0.35	0.55	0.45
Sunday	45	35	10	5	0.40	0.33	0.60	0.55

The battery capacity of an EV is 0.04 MWh and the average arrival energy content, SOC, is 50%. The rated charging/discharging capacity of the V2G stations,  $CH^{max}$ , is 0.02 MWh. The maximum and minimum allowed SOC of an EV's battery is 0.9 and 0.1, respectively. The cost of battery wear,  $\gamma$ , is assumed to be 10 (\$/MWh).

### 3.7.3 Day-ahead energy prices and power distributor

The energy prices of year 2010 to year 2015 collected from [25] are assumed to be the forecasted prices for the study intervals in the planning horizon. The weekly energy prices in

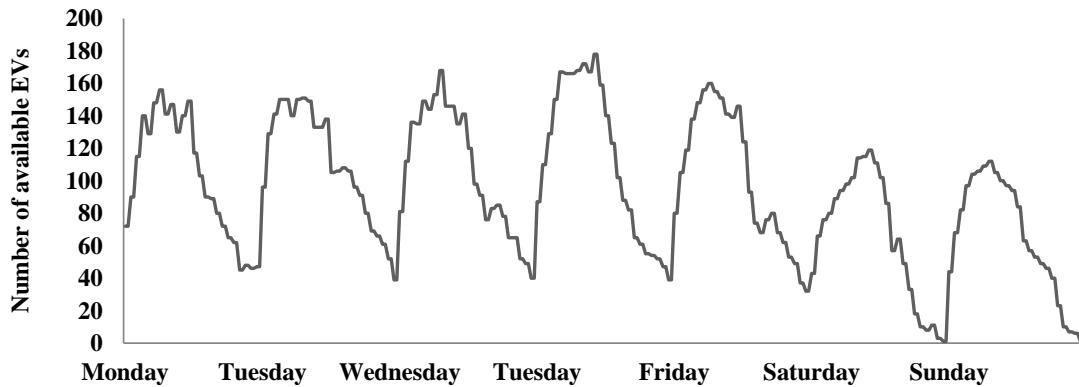


**Figure 3.2:** One scenario for the available EVs in the parking during a week in spring

spring are given in Figure 3.3. For the real-time transactions, the microgrid imports energy at a cost of 150 (\$/MWh) and exports it at a price of 5 (\$/MWh).

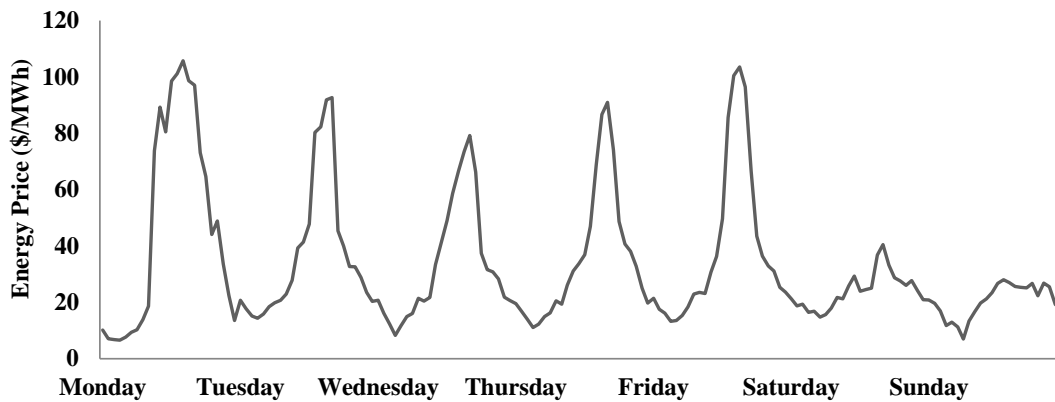


**Figure 3.3:** Energy price in the day-ahead during a week in spring

### 3.7.4 Net Demand Uncertainty

The Monte Carlo simulation is used to generate scenarios for representing the uncertainties in demand, wind energy and solar energy. As the solar and wind energy sources are assumed to be non-dispatchable, the net demand scenarios at each hour are obtained by subtracting the wind and solar energy output from the demand at that hour. To generate the scenarios, we use a truncated multivariate normal distribution (TMVN) [24]. The probability density function of TMVN is given in (22) [25]. The covariance matrix,  $\Sigma$ , represents the between hour interdependency.

$$f(x, \mu, \Sigma, a, b) = \frac{\exp(-1/2(x - \mu)^T \Sigma^{-1} (x - \mu))}{\int_a^b \exp(-1/2(x - \mu)^T \Sigma^{-1} (x - \mu)) dx} \quad (3.4)$$

To estimate the parameters of the TMVN, we use wind and solar energy output data provided by the renewables integration study datasets in [26]. We also collected historical hourly demand data from [25]. We generate 1000 net demand scenarios for one week and reduced them to 10 scenarios using the K-means clustering algorithm. In Figure 3.4, we show three of the net demand scenario for one week from the spring season of year one. We assumed an increases rate of 8% for the demand from one year to the next.

## 3.8 Simulation Results

We run all simulations on a 2.8 GHz Core 2Duo processor with 4GB of memory for a planning horizon of five years. To compute the total operation cost for a given number of V2G stations, we solve the operation problem 20 times (4 seasons by 5 years) for weekly intervals (168 hours). As we consider 10 scenarios for the net load and 10 scenarios for the parked EVs, the problem is solved for 100 scenario combinations. The purchasing cost of a V2G station and the annual interest rate are assumed to be \$5k and 5%, respectively.

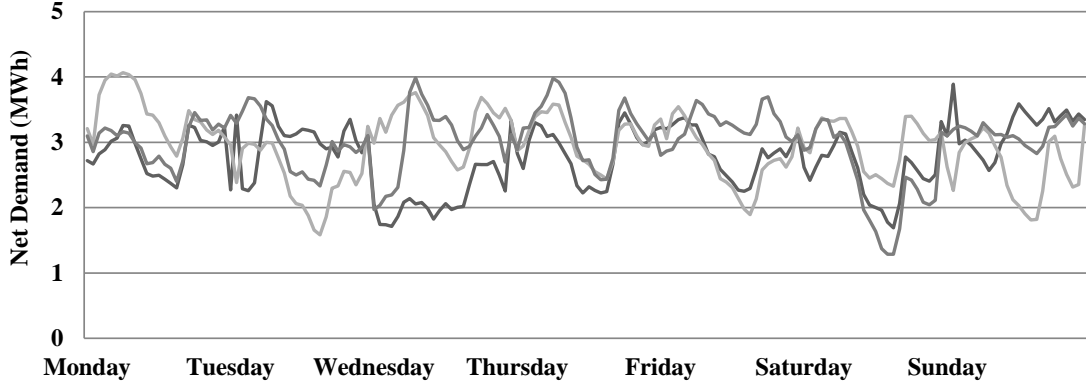


**Figure 3.4:** Three of the net demand scenario for one week from the spring season of year one

We start the Nelder-Mead algorithm with  $n_1=100$  and  $n_2=500$  V2G stations. Figure 3.5 shows the convergence of the Nelder-Mead algorithm. The algorithm converges after 15 iterations. The converged solution is 320 V2G stations with a total cost of \$10,755k. In Table 3.2, we provide the expected OC for one week of a season within a year. The table also shows the expected OC for a season within a year and the entire year. Results for 100 and 500 V2G stations are shown in Tables 3.3 and 3.4.

**Table 3.2:** Investment and operation costs for 320 V2G

Year	Expected OC (Weekly) (\$)				Expected OC(Seasonally) (\$)=13 Weekly OC				Total OC(\$)	IC (\$) 320 V2G	Total cost PW (\$)
	Spring	Summer	Fall	Winter	Spring	Summer	Fall	Winter			
1	36,819	38,290	36,484	36,709	478,642	497,770	474,295	477,221	1,927,929	1.6M	10,755,336
2	38,002	39,086	36,899	37,572	494,024	508,112	479,692	488,437	1,876,443		
3	38,852	39,930	37,895	38,837	505,081	519,096	492,635	504,877	1,833,731		
4	39,168	40,944	38,953	39,882	509,185	532,271	506,392	518,468	1,784,962		
5	39,272	41,876	39,983	40,838	510,530	544,393	519,773	530,890	1,732,271		
Total	192,112	200,126	190,214	193,838	2,497,461	2,601,643	2,472,788	2,519,893	9,155,336		

**Table 3.3:** Investment and operation costs for 100 V2G

Year	Expected OC (Weekly) (\$)				Expected OC(Seasonally) (\$)=13 Weekly OC				Total OC(\$)	IC (\$) 320 V2G	Total cost PW (\$)
	Spring	Summer	Fall	Winter	Spring	Summer	Fall	Winter			
1	44,619	45,951	43,264	44,731	580,043	597,361	562,437	581,499	2,321,340	0.5M	11,596,409
2	45,962	47,205	44,608	45,825	597,505	613,671	579,899	595,728	2,273,146		
3	47,151	48,069	45,809	47,250	612,966	624,891	595,520	614,247	2,220,067		
4	48,427	49,387	46,926	48,168	629,548	642,033	610,037	626,187	2,166,337		
5	49,401	50,463	48,295	49,643	642,209	656,022	627,836	645,362	2,115,520		
Total	235,559	241,075	228,902	235,617	3,062,271	3,133,977	2,975,729	3,063,024	11,096,410		

**Table 3.4:** Investment and operation costs for 500 V2G

Year	Expected OC (Weekly) (\$)				Expected OC(Seasonally) (\$)=13 Weekly OC				Total OC(\$)	IC (\$) 320 V2G	Total cost PW (\$)
	Spring	Summer	Fall	Winter	Spring	Summer	Fall	Winter			
1	34,040	35,305	33,640	34,031	442,520	458,965	437,320	442,403	1,781,208	2.5M	11,023,187
2	35,131	36,222	34,298	35,010	456,703	470,886	445,874	455,130	1,741,517		
3	36,007	37,001	35,216	36,176	468,091	481,013	457,808	470,288	1,702,676		
4	37,032	38,119	36,100	37,140	481,416	495,547	469,300	482,820	1,666,414		
5	38,210	38,887	37,416	38,021	470,730	505,531	486,408	494,273	1,631,371		
Total	178,420	185,534	176,670	180,378	2,345,460	2,411,942	2,296,710	2,344,914	8,523,187		

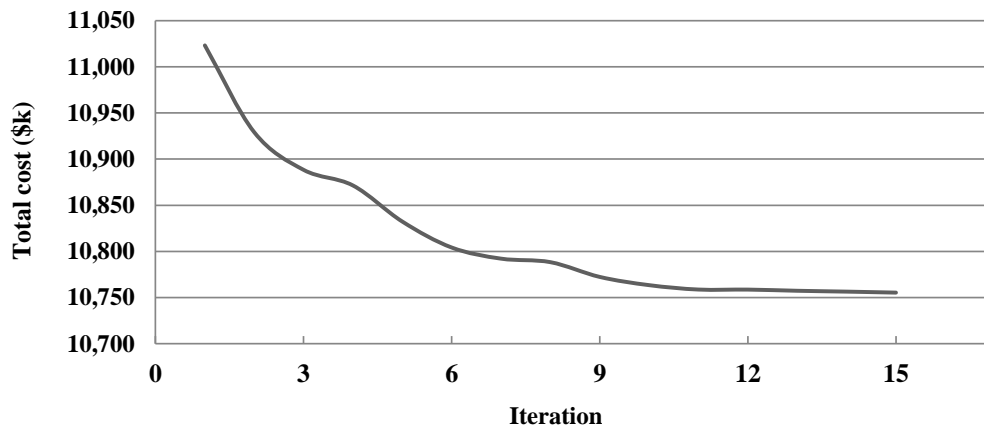


**Figure 3.5:** The convergence of the Nelder-Mead algorithm

### **3.8.1 Effect of the V2G technology**

To show the effect of investing on the V2G technology, we set the number of V2G stations to zero to simulate that the V2G technology is not present and compare the results with the case where 320 V2G stations are installed in the parking facility. The total operation cost of the microgrid over the 5-year planning horizon is \$12,843k which is \$2,092k more than having 320 stations in the parking facility.

### **3.8.2 Payback Period**

The difference between the annual cost savings and the initial investment is referred as the discounted project balance. The discounted payback period is the number of years required to recover the initial investment in a project. Figure 3.6 shows the discounted payback period, which is 3 years, for 320 V2G stations. The project balance from the start until year 3 is negative which indicates the amount of loss if the project is terminated at any point before year 3. After year 3, the project balance becomes positive which indicates the amount of cash that directly contributes to the final profitability of the investment.

### **3.8.3 Effect of uncertainty**

As we have considered the uncertainty of the net load and the number of parked EVs, we assess the effect of these two uncertainty sources. We solve the problem with 320 V2G station considering only one scenario for each stochastic parameter. The scenario is obtained by averaging the 10 scenarios of each parameter. The total cost of the solved problem is \$11,195k which is \$445k higher than that of the stochastic problem with 100 scenarios. The discounted payback period of the one scenario case is four years. The total cost is calculated by determining the first stage decision variables and then using them to obtain the second stage decisions for each of the 100 scenarios. The total cost is obtained by averaging the operation costs of each scenario.

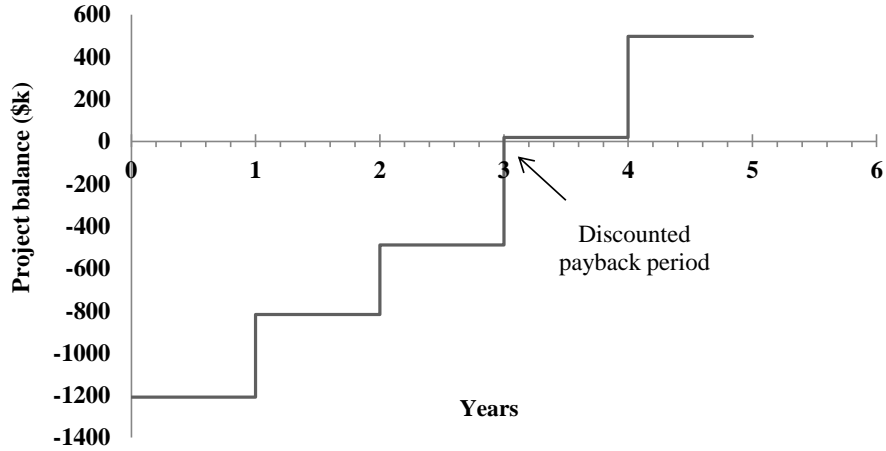


**Figure 3.6:** Discounted payback period considering investment on 320 V2G stations

### 3.9 Conclusions

In this chapter, we proposed an optimal investment model to upgrade a microgrid parking facility with V2G technology. The microgrid included different sources of energy generation and was set to use the parking facility as an energy storage resource. To model the variable storage capacity of the parking facility, we used an inhomogeneous continuous time Markov chain, and to model the uncertainties, we used the Monte Carlo simulation. A two stage stochastic programming framework was proposed to formulate the optimization problem that aimed to determine the optimal investment on the V2G technology. To solve the problem, we divided it into operation and investment sub problems. The Benders decomposition was used to solve the operation problem for weekly intervals and the Nelder-Mead algorithm to find the optimal solution for the V2G stations in the parking facility. We tested the proposed model on a 14-bus distribution system for a planning horizon of five years. The simulation results showed that investing on the V2G technology in the parking facility reduces the microgrid’s cost of electricity supply in the long run. We also showed the

superiority of the stochastic model to the deterministic model, and assessed the economic payback period for investing on the V2G technology.

## References

- [1] A. S. Masoum, S. Deilami, P.S. Moses, M.A. Masoum, and A. Abu-Siada, "Smart load management of plug-in electric vehicles in distribution and residential networks with charging stations for peak shaving and loss minimization considering voltage regulation" *IET Generation, Transmission and Distribution*, vol. 5, no. 8, pp. 877-888, 2011.
- [2] J. A. P. Lopes, F.J. Soares, and P. M. R. Almeida, "Integration of electric vehicles in the electric power system", *Proceedings of the IEEE*, vol. 99, no. 1, pp. 168-183, 2011.
- [3] S. Deilami, , A.S. Masoum, P.S. Moses, and M.A. Masoum, "Real-time coordination of plug-in electric vehicle charging in smart grids to minimize power losses and improve voltage profile", *IEEE Transactions on Smart Grid*, vol. 2, no. 3, pp. 456-467, 2011.
- [4] R. Sioshansi, and P. Denholm, "Emissions impacts and benefits of plug-in hybrid electric vehicles and vehicle-to-grid services", *Environmental science and technology*, vol. 43, no.4, pp. 1199-1204, 2009.
- [5] S. B. Peterson, J.F. Whitacre, and J. Apt , "The economics of using plug-in hybrid electric vehicle battery packs for grid storage" *Journal of Power Sources*, vol. 195 no.8, pp. 2377-2384, 2010.
- [6] Z. Wang, and S. Wang S , "Grid power peak shaving and valley filling using vehicle-to-grid systems", *IEEE Transactions on Power Delivery*, vol. 28, no. 3, pp. 1822-1829, 2013.
- [7] K. Mets, T. Verschueren, W. Haerick, C. Develder, and F. De Turck, "Optimizing smart energy control strategies for plug-in hybrid electric vehicle charging", *IEEE In Network Operations and Management Symposium Workshops* pp. 293-299 . 2010.

- [8] C. Chen, S. Duan, “Optimal integration of plug-in hybrid electric vehicles in microgrids”, *IEEE Transactions on Industrial Informatics*, vol. 10, no. 3, pp. 1917-1926, 2014.
- [9] Clement-Nyns, K., Haesen, E., and Driesen, J, “The impact of charging plug-in hybrid electric vehicles on a residential distribution grid”, *IEEE Transactions on Power Systems*, vol. 25, no. 1, pp. 371-380, 2010.
- [10] M. Gonzalez Vay and G. Andersson, “Optimal Bidding Strategy of a Plug-In Electric Vehicle Aggregator in Day-Ahead Electricity Markets Under Uncertainty”, *IEEE Transactions on Power Systems*, vol. 99, pp. 1-11, 2014.
- [11] M. Gonzalez Vay and G. Andersson, “Centralized and decentralized approaches to smart charging of plug-in vehicles”, *IEEE General Meeting In Power and Energy Society*, 2012.
- [12] L. Jia, L., Z. Hu, Y. Song and Z. Luo, “Optimal siting and sizing of electric vehicle charging stations”, *IEEE International In Electric Vehicle Conference*, pp. 1-6, 2012.
- [13] Z. Liu, F. Wen and G. Ledwich, “Optimal planning of electric-vehicle charging stations in distribution systems”, *IEEE Transactions on Power Delivery*, vol. 28 no. 1, pp. 102-110. 2013.
- [14] F. Fazelpour, M. Vafaeipour, O. Rahbari and M. A. Rosen, “Intelligent optimization to integrate a plug-in hybrid electric vehicle smart parking lot with renewable energy resources and enhance grid characteristics”, *Energy Conversion and Management*, vol. 77, pp. 250-261, 2014.
- [15] E. Mortaz and J. Valenzuela, “Microgrid energy scheduling using storage from electric vehicles”. *Electric Power Systems Research* Vol. 143, pp. 554562, 2016.
- [16] J. C. Lagarias, J. A. Reeds, M. H. Wright, M. H., and P. E. Wright, “Convergence properties of the Nelder-Mead simplex method in low dimensions, *SIAM Journal on optimization*, vol. 9, no. 1, pp 112-147, 1998.

- [17] J. Valenzuela and J. Wang, “A probabilistic model for assessing the long-term economics of wind energy”, *Electric Power Systems Research*, vol.81, no.4, pp. 853-861, 2011.
- [18] Q.H. Zhao, D. Urosevi, N. Mladenovi, and P. Hansen, “A restarted and modified simplex search for unconstrained optimization”, *Computers and Operations Research*, vol. 36, no. 12, pp. 3263-3271, 2009.
- [19] H. Khodr, J. Martinez-Crespo, M. Matos ,and J. Pereira, “Distribution systems reconfiguration based on OPF using Benders decomposition”, *IEEE Transactions on Power Delivery*, vol. 24, no. 4, pp. 2166-2176, 2009.
- [20] M. Gay, “IBM ILOG CPLEX Optimization Studio CPLEX User’s Manual”, *International Business Machines Corporation*, vol. 12, 2012.
- [21] R. D. Zimmerman, C. Murillo-Sanchez, and R. Thomas, “Matpower: Steady-State Operations, Planning and Analysis Tools for Power Systems Research and Education”, *IEEE Transactions on Power Systems*, vol. 26, no. 1, pp. 12-19, 2011.
- [22] P. Buchholz, and I. Schulz, “Numerical analysis of continuous time Markov decision processes over finite horizons”, *Computers and Operations Research*, vol. 38, no. 3, pp. 651-659, 2011.
- [23] Y.F. Li, Y.H Lin. and E Zio., “Stochastic modeling by inhomogeneous continuous Markov chain”, *EURO Workshop on Stochastic Modeling*, 2012.
- [24] L. Baringo, and A. Conejo, “Correlated wind-power production and electric load scenarios for investment decisions”, *Applied Energy*, vol. 101, pp. 475-482, 2013.
- [25] PJM, “Analysis”, 2014. [Online]. Available: <http://www.pjm.com>.
- [26] Wilhelm S. Wilhelm and B. Manjunath, tmvtnorm: A package for the truncated multivariate normal distribution, *sigma 2*, vol. 2, 2010.

[27] NREL NREL, “The Dynamic Maps, GIS data and Analysis Tools”, 2014. [Online].  
Available: *http : //www.nrel.gov/gis/datawind.html*.